UNIVERSITY OF CALIFORNIA, SAN DIEGO

Observations and Modeling of Southern California Beach Sand Level Changes

A dissertation submitted in partial satisfaction of the

requirements for the degree Doctor of Philosophy

in

Oceanography

by

André D. Doria

Committee in charge:

Professor R.T. Guza, Chair
Professor Clint Winant, Co-Chair
Professor C. F. Driscoll
Professor Sarah T. Gille
Professor Myrl Hendershott

2016

The dissertation of André D. Doria is approved, and it is acceptable in quality and form for publication on microfilm and electronically:

_____

_____

_____

_____
Co-Chair

_____
Chair

University of California, San Diego

2016

EPIGRAPH

"All that is gold does not glitter,
Not all those who wander are lost;"

J. R. R. Tolkien

"It doesn't matter how beautiful your theory is, it doesn't matter how smart you are. If it doesn't agree with experiment, it's wrong."

"Nobody ever figures out what life is all about, and it doesn't matter. Explore the world. Nearly everything is really interesting if you go into it deeply enough."

Richard Feynman

TABLE OF CONTENTS

LIST OF FIGURES

LIST OF TABLES

ACKNOWLEDGEMENTS

I would like to recognize Luc Lenain, Professor Ken Melville, and Professor Thomas Murphy for their support throughout my undergraduate and initial graduate program endeavors. I am deeply grateful for their assistance. I would like to acknowledge Professor Robert Guza for his support and guidance as my advisor and the chair of my committee throughout the majority of my graduate program tenure. I have profound gratitude towards the members of Guza's engineering staff, both past and present (Bill Boyd, Brian Woodward, Kent Smith, Dennis Darnell, Rob Grenzeback, and Zoe Dagan), Bill O'Reilly, the CDIP (Coastal Data Information Program) staff, as well as my committee members (Clint Winant, Myrl Hendershott, Sarah Gille, and Fred Driscoll). Without their substantial efforts and duty, this dissertation would not exist. Lastly, I would like to recognize five individuals that provided me encouragement and demanding scientific, mathematical, and analytical instruction during my nascent years of scientific curiosity. Their influence motivated me to leave the manual labor workforce to pursue physics, a subject extremely remote to me at the time, but even now, many years later, continues to bring me delight. Patty Anderson, Takashi Nakajima, Monika Brannick, Al Trujillo, and Patty Dean, I thank you.

The text of Chapter 1, in full, is a reprint with minor modifications of the paper "Estimating Changes in Near-Shore with Subaerial Surveys," *Journal of Atmospheric and Oceanic Technology*, 30, 2225–2232, doi: 10.1175/JTECH-D-13-00012.1

(Copyright of the American Meteorological Society 2013). The dissertation author was the primary researcher and first author with guidance provided by R.T. Guza.

The text of Chapter 2, in full, is a reprint with minor modifications of the paper "Observations and modeling of San Diego beaches during El Niño," *Continental Shelf Research*, 124, 153-164, http://dx.doi.org/10.1016/j.csr.2016.05.008 (Copyright of Elsevier Ltd. 2016). The dissertation author was the primary researcher and first author with guidance provided by R.T. Guza, M. L. Yates, and William C. O'Reilly.

The text of Chapter 3, in full, is a reprint with minor modifications of the paper "Regional variability and modeling of Southern California beach sand levels during El Niño," submitted for publication to the *Continental Shelf Research*. The dissertation author was the primary researcher and first author with guidance provided by R.T. Guza and William C. O'Reilly.

VITA

2006	A.A., Mathematics A.A., Liberal Arts and Sciences Palomar College
2007	B.S., Physics (Summa Cum Laude) University of California, San Diego
2008-2014	Research Assistant University of California, San Diego
2010	M.S., Oceanography University of California, San Diego
2016	Ph.D., Oceanography University of California, San Diego

PUBLICATIONS

Barnard, P. L., J. Allan, J. E. Hansen, G. M. Kaminsky, P. Ruggiero, and A. Doria, 2011: The impact of the 2009–10 El Niño Modoki on U.S. West Coast beaches, *Geophys. Res. Lett.*, 38, L13604, doi:10.1029/2011GL047707.

Doria, A., and R. T. Guza, 2013: Estimating Changes in Near-Shore Bathymetry with Subaerial Surveys, *J. Atmos. Oceanic Technol.*, 30, 2225–2232, doi: http://dx.doi.org/10.1175/JTECH-D-13-00012.1.

Barnard, Patrick L., Andrew D. Short, Mitchell D. Harley, Kristen D. Splinter, Sean Vitousek, Ian L. Turner, Jonathan Allan, Massayuki Banno, Karin R. Bryan, Andre Doria, Jeff E. Hansen, Shigeru Kato, Yoshiaki Kuriyama, Evan Randall-Goodwin, Peter Ruggiero, Ian J. Walker, and Derek K. Heathfield, 2015: Coastal vulnerability across the Pacific dominated by El Niño/Southern Oscillation. *Nature Geoscience*, 8, 801-807, doi:10.1038/ngeo2539

Doria, A., R.T. Guza, William C. O'Reilly, and M. L. Yates, 2016: Observations and modeling of San Diego beaches during El Niño. *Continental Shelf Res.*, 124, 153-164, http://dx.doi.org/10.1016/j.csr.2016.05.008.

Doria, A., R.T. Guza, and William C. O'Reilly, 2016: Regional variability and modeling of Southern California beach sand levels. *Continental Shelf Res.*, submitted for publication.

FIELDS OF STUDY

Major Field: Oceanography (Physical Oceanography)

Studies in Fluid Mechanics:
Professors Myrl Hendershott and Joel Norris

Studies in Waves:
Professors Clint Winant and R. T. Guza

Studies in Applied Mathematics:
Professors Glenn Ierley, Stefan G. Llewellyn-Smith, and William R. Young

Studies in Data Analysis:
Professors Dan Rudnick, Sarah Gille, Duncan Agnew, Cathy Constable, Bob Parker, and Jay Barlow

ABSTRACT OF THE DISSERTATION

Observations and Modeling of Southern California Beach Sand Level Changes

by

André D. Doria
Doctor of Philosophy in Oceanography
University of California, San Diego, 2016
Professor R. T. Guza, Chair
Professor Clint Winant, Co-Chair

Repeated aerial and ground-based observations that measured seasonal beach sand level changes along 195 km of coastline for up to 16 years were used to characterize and model Southern California beach sand level changes. A wave buoy network initialized a spectral refraction wave model that provided nearshore (~10 m depth) hourly wave estimates every ~100 m alongshore throughout the entire study region. Localized and regional biannual ground-based surveys captured seasonal subaerial beach profile changes across San Diego County, as well as the associated bathymetry changes not detected by aerial methods. Volume changes along the surveyed bathymetry transects varied seasonally owing to fluctuations in the incident

wave energy. Comparative analysis of the volume changes along the beach profiles demonstrated estimating the fraction of subaqueous volume change based exclusively on subaerial observations is highly variable with a reduction in the total volume change captured by the subaerial observations particularly during periods of excessive erosion. Notably, the link between near-shore the displaced beach face sand volume (e.g. both subaerial and bathymetric profile components) and that of the subaerial beach is obscure.

Observations at five focus sites in San Diego County characterized short-term and long-term shoreline changes and waves, including the impacts of two significant El Niño winters, from 1997 through 2013. An existing wave-driven shoreline model accurately predicted shoreline fluctuations during years of normative wave and beach conditions, but over-predicted erosion during remarkable erosion events such as El Niño. Modifications to the model formulation account for erosion resistant features such as non-erodible seawall back beaches or durable strata (e.g. cobbles) exposed during severe erosion. This improved the model skill (i.e. data to model correlation R^2) during highly erosive wave events.

High spatial resolution biannual aerial lidar surveys captured regional beach sand level changes spanning the entire 195-km study region. Alongshore variations in both waves and beach sand levels were notable with distinct large-scale differences occurring between the northern and southern halves of the study site. Additional ground-based data were used conjointly with the aerial observations to tune a regional shoreline model spanning 90 km of San Diego County coast.

1

Estimating changes in near-shore bathymetry with subaerial surveys

1.1 Abstract

Surveys of the subaerial beach (e.g. landward of approximately the Mean Sea Level (MSL) depth contour) are widely used to evaluate temporal changes in sand levels over large alongshore reaches. Here, seasonal beach face volume changes based on full bathymetry beach profiles (to ~8 m depth) are compared with estimates based on the subaerial section of the profile. The profiles span 15 years and 75 km of southern California shoreline, where seasonal vertical fluctuations in nearshore sand levels of a few meters are common. In years with relatively low winter wave energy, most erosion occurs above the MSL contour, and subaerial surveys capture as much as 90% of the total (relatively small) seasonal beach face volume change. In response to more energetic winter waves, beach face erosion increases and occurs as deep as 3 m

below MSL, and subaerial surveys capture as little as 10% of the total beach face volume change. Patchy, erosion resistant rock and cobble layers contribute to alongshore variation of the subaerial fraction of beach face volume change.

1.2 Introduction

Beach sand levels, important to coastal management and risk assessment, vary over a wide range of spatial and temporal scales (Nicholls et al., 2007; Long et al., 2011; Yang et al., 2012). Changes in subaerial sand levels over large alongshore spans (many 10s of km) are often characterized using airborne lidar observations (Sallenger et al. 2002). Surveys are optimally collected at low tide, maximizing the amount of subaerial beach face measured, and Mean Sea Level (MSL) is typically the deepest contour surveyed. Errors in the estimated vertical sand levels, typically ~15 cm root-mean-square, are small compared with the O(1 m) topographic changes associated with large individual storms (Sallenger et al., 2003). Recently, airborne lidar surveys have been used to compare the impacts of El Niños on U.S. West Coast beaches (Barnard et al., 2011; Revell et al., 2011). Subaerial surveys obtained with ground-based lidar and GPS-equipped vehicles are widely used to characterize nearshore sand volume changes over shorter alongshore spans of a few kilometers, but with increased frequency relative to airborne lidar. Subaerial volumes by definition exclude changes below the waterline (nominally MSL). Farris and List (2007) show that changes in "beach width" (e.g. in the cross-shore location of the MSL depth contour) are well correlated with, and a convenient proxy for, subaerial volume change. However, the relationship between subaerial and subaqueous volume changes in unclear. Here,

seasonal volume changes above MSL are compared with estimates using profiles extending to ~8 m depth.

1.3 Observations

1.3.1 Study site

The 75 km long San Diego County study region includes wide (100-200 m) sandy beaches backed by low-lying sandy dunes or lagoon mouths, and narrow beaches backed by sedimentary sea-cliffs (Moore et al., 1999; Young et al., 2010) (Figure 1.1). Most San Diego beaches are low sloped, with a northward trend of increasing beach slope (0.02 to 0.05) and increasing mean sediment size (0.15-0.29 mm) (Yates et al., 2009b).

1.3.2 Bathymetric surveys

Bathymetric surveys at Torrey Pines Beach (semi-annual: winter and summer, 2004-2010) are on ~100 m alongshore spaced shore-normal transects (Figure 1.1) extending from the back beach to at least 6 m below MSL (Yates et al., 2009a,b). Subaerial and wading depth surveys were collected at low tide using a GPS-equipped all-terrain vehicle (ATV) and pushcart. At high tide, subaqueous sand levels were measured using a GPS-equipped personal watercraft with an acoustic depth sounder (Seymour et al., 2005).

Sand levels throughout San Diego County were surveyed semi-annually (e.g. fall and spring) for 15 years (1996-2010). These surveys extended to ~8 m depth with an Corporation 1997-2010). The surveys are broadly representative of accreted

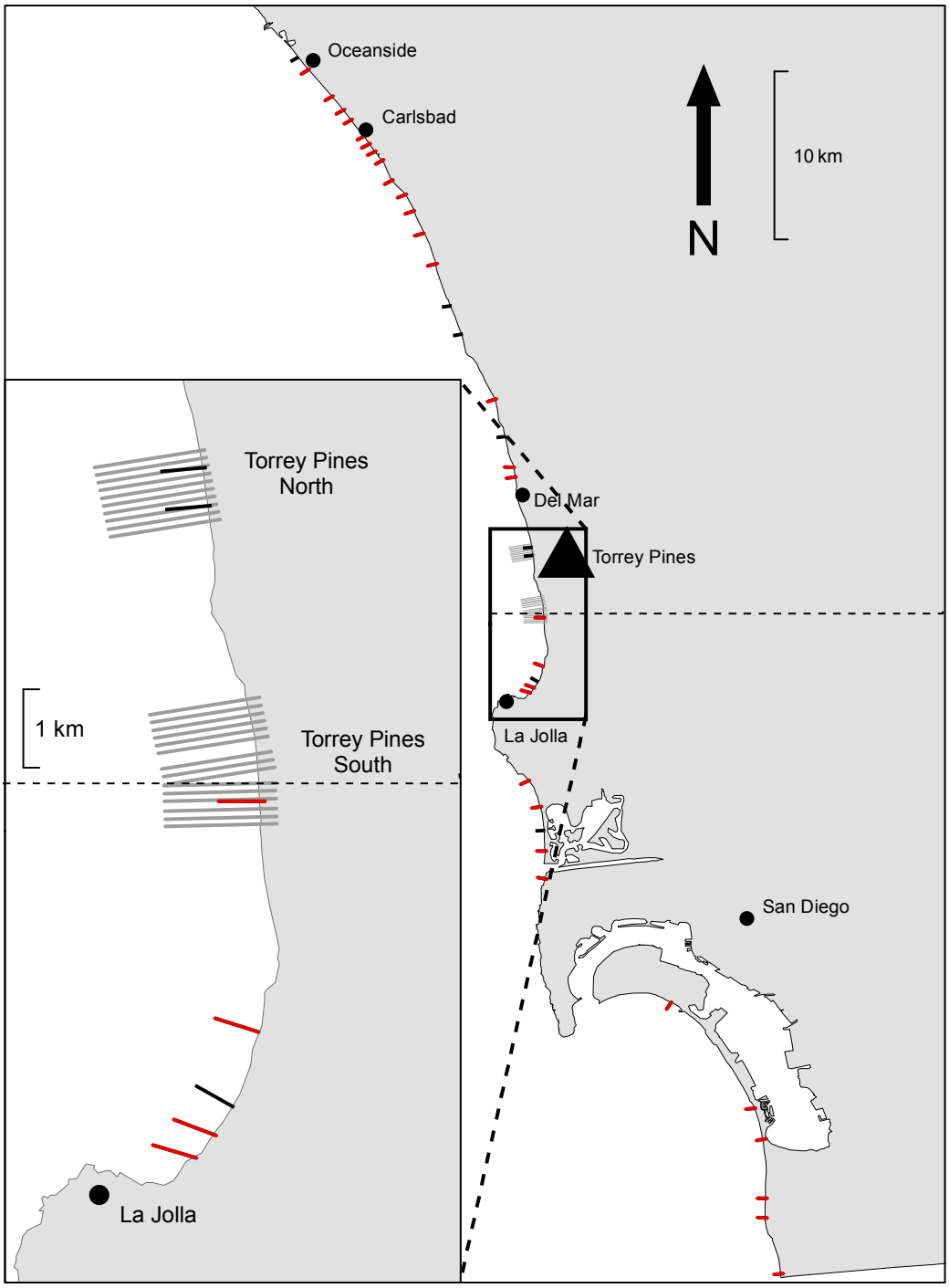

Figure 1.1: Map of study region: 38 cross-shore transects (each with at least 20 surveys) span 75 km of San Diego County (red and black markers). Red lines indicate transects with a statistically significant R^2 (see Figure 1.6 caption). Torrey Pines focus site (25 transects) is shown in the inset (grey markers). The thin dashed horizontal black line indicates the midpoint separating north from south San Diego.

summer and eroded winter profiles, and usually do not correspond to the seasonal extrema (see Appendix A).

1.3.3 Beach face volume and beach face depth estimation

Sand level data were gridded every 1 m in the cross-shore direction along shore-normal lines using a 2 m running mean. Transects with cross-shore data gaps greater than 20 m or low overall data coverage (<30%) were discarded. The cross-shore integrated volume change, ΔVol, between temporally consecutive, gridded cross-shore profiles (Figure 1.2a) is

$$\Delta Vol(X_{trunc}) = \int_{X_{trunc}}^{X_{bb}} \left(h_{i+1}(x) - h_i(x)\right) dx , \qquad (1.1)$$

where $h(x)$ is the sand level, subscript i is the temporal survey index, X_{bb} is the fixed location of the back beach, and X_{trunc} is the off-shore integration limit. For a subaerial survey $X_{trunc} = X_{MSL}$, the location of the MSL depth contour (Figure 1.2a). The cross-shore boundary X_{bface} separates regions of erosion from accretion, and is the cross-shore location where (1.1) has a global extrema (e.g. $X_{trunc} = X_{bface}$)(Figure 1.2b). The depths at X_{trunc} and X_{bface} are h_{trunc} and h_{bface}. Each pair of consecutive seasonal profiles yields values of X_{bface} and h_{bface} (Figure 1.2a).

The effect of truncating transects on volume change estimates was quantified by varying the seaward limit of volume change between h_{bface} (where all beach face change is captured) to above MSL (Figure 1.2b). The fraction of ΔVol_{bface} captured

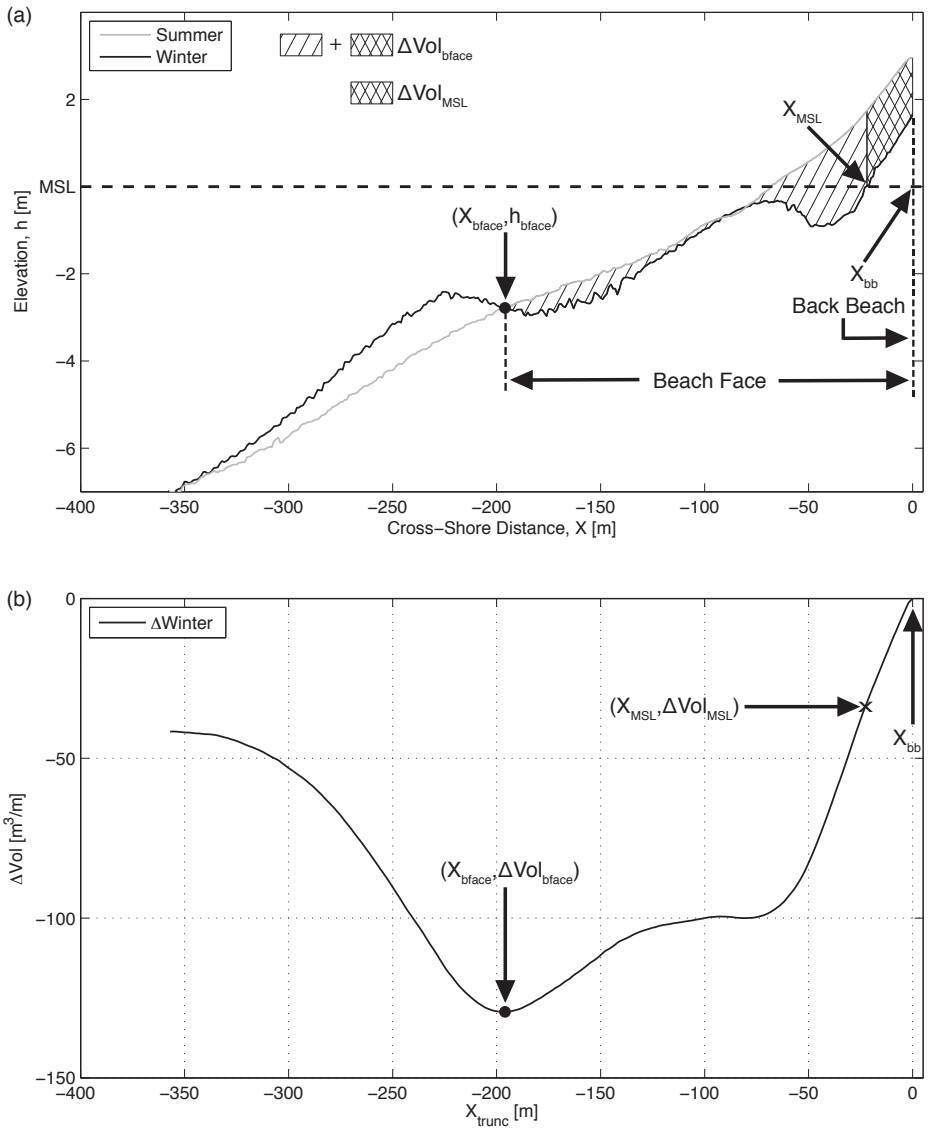

Figure 1.2: (a) Depth profiles extend from the back beach about 350 m to depth h = MSL-7 m. The beach face boundary, X_{bface}, at depth h_{bface}, separates depth changes of opposite sign. With the summer profile preceding the winter profile, hatched areas correspond to erosion. A winter sandbar is formed seaward of X_{bface}. (b) ΔVol (1) is maximum at $X_{trunc} = X_{bface}$. A subaerial survey, extending as far seaward as MSL on the eroded profile, captures only ~0.25 of the total beach face erosion (e.g. $\lambda_{MSL} = 0.25$).

with a truncated survey is

$$\lambda_{trunc} = \frac{\Delta Vol(h_{trunc})}{\Delta Vol(h_{bface})}. \quad (1.2)$$

1.4 Results

A single transect at Torrey Pines (Figure 1.3) illustrates a general seasonal beach profile behavior. Large seasonal beach face volume change extends further offshore, and to deeper depths, than small seasonal changes (Figure 1.3; compare cross-shore locations and depths of circles in the left panels with the right panels). With a small beach face volume change, λ_{MSL} is larger than with a large beach face volume change.

The 10 transects at North Torrey Pines exhibit similar patterns of seasonal change. Seasonal beach face volume changes ΔVol_{bface}, integrated from the back beach to X_{bface} (1.1), vary between about 50 and 250 m^3/m (Figure 1.4a). Beach face change always extended below MSL, and h_{bface} varied between about -0.5 and -4 m (Figures 1.4a, 1.5c,d). Subaerial surveys on average capture 40% of the total volume change (average $\lambda_{MSL} = 0.4$), but the variation of λ_{MSL} is large (Figure 1.4b). Low λ_{MSL} tends to occur with large seasonal volume changes, regardless of season (Figure 1.5e). Combined South San Diego transects (locations of significant R^2 in Figure 1.6; where R^2 is defined as $\left(\frac{\langle xy \rangle}{\sigma_x \sigma_y}\right)^2$) are similar to North Torrey Pines (compare left with

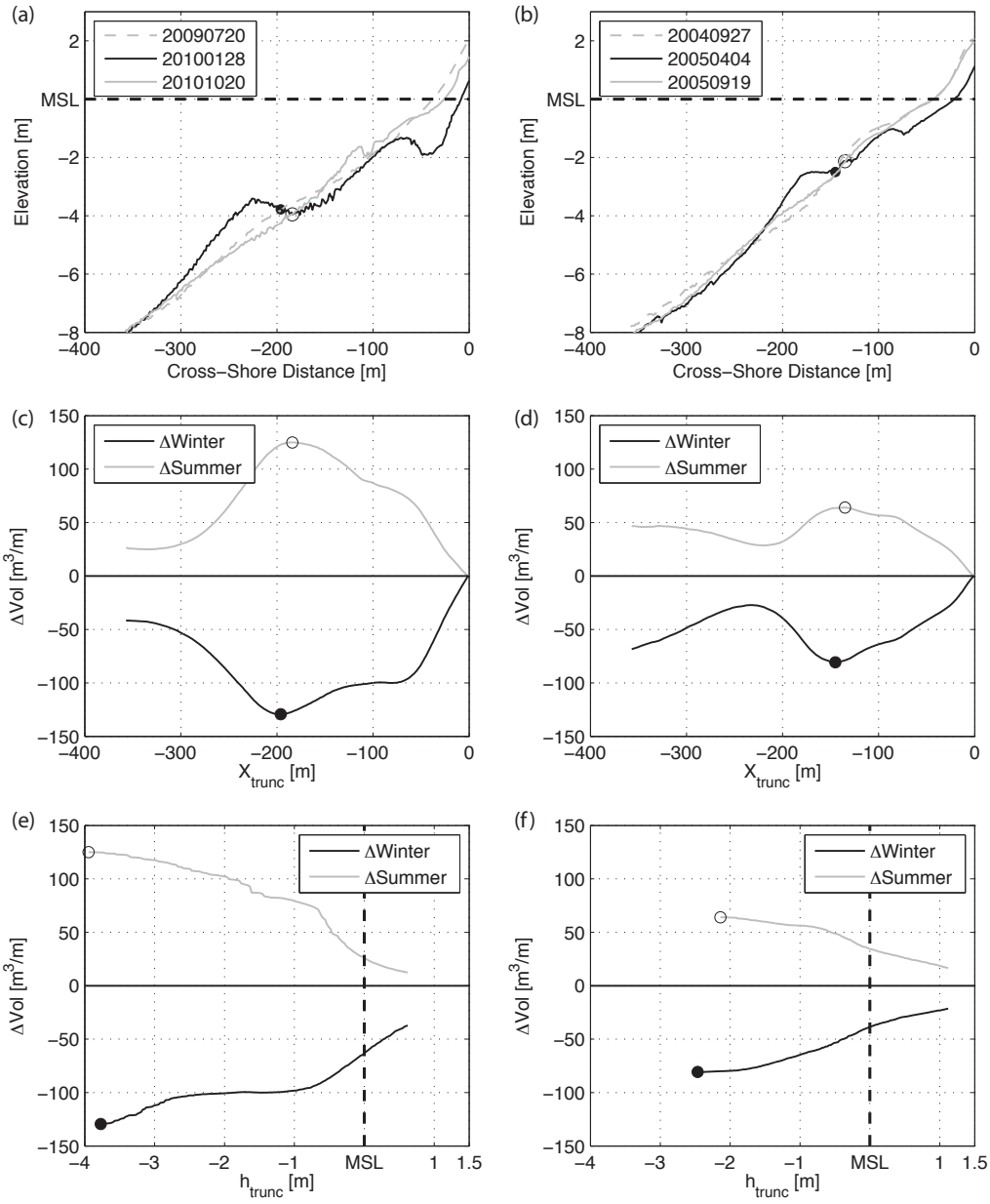

Figure 1.3: Seasonal sand level changes on the same transect at Torrey Pines for years with relatively large (left) and small (right) profile changes. (a),(b) Elevation versus cross-shore distance. Black (gray) curves are winter (summer) profiles. (c),(d) ΔVol versus location of cross-shore truncation X_{trunc}. Gray is change from winter to summer ($\Delta Summer$), and black is summer to winter ($\Delta Winter$). Circles (a)-(d) are the seaward limit of beach face change, X_{bface}. (e),(f) ΔVol versus h_{trunc}, with $h_{trunc} \geq h_{bface}$ (circles indicate $h_{trunc} = h_{bface}$).

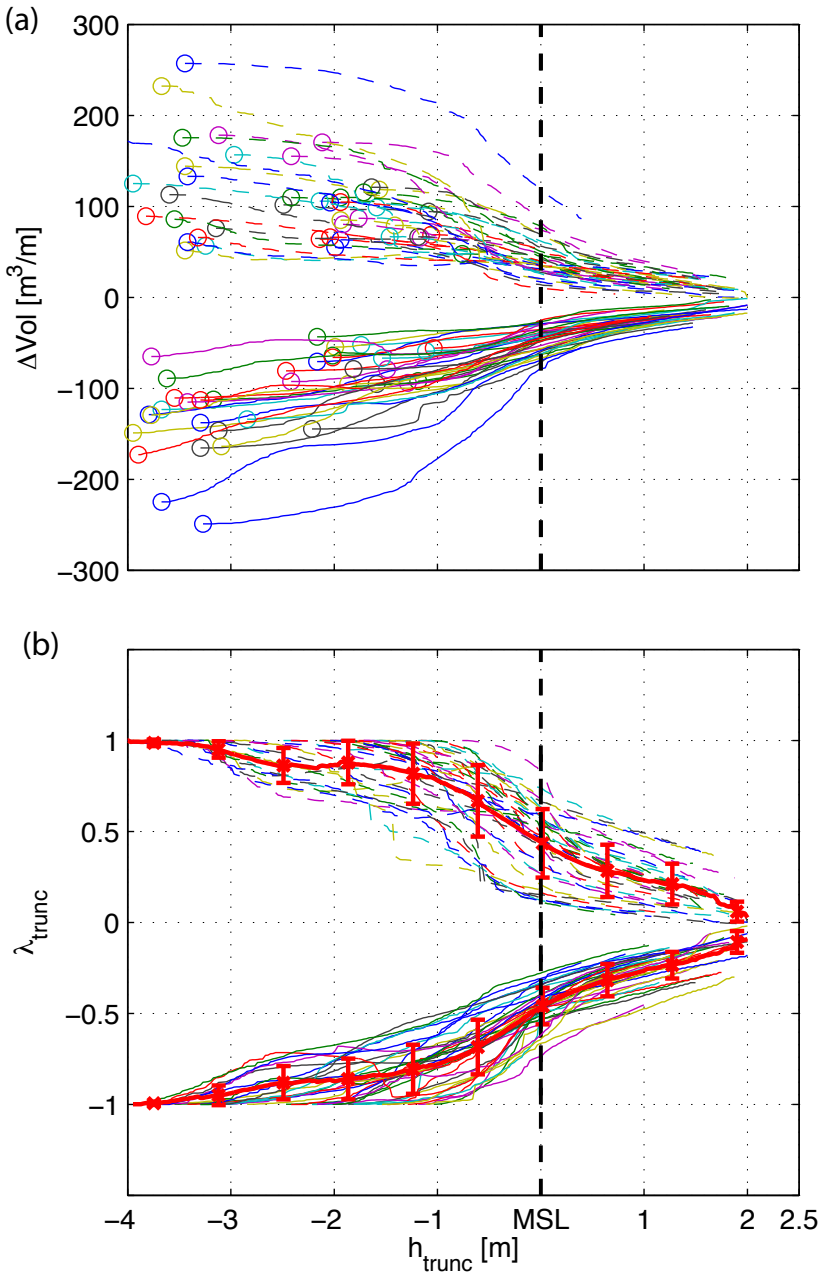

Figure 1.4: Seasonal beach volume changes for all 10 North Torrey Pines transects: (a) ΔVol and (b) λ_{trunc} both versus h_{trunc}, with $h_{trunc} \geq h_{bface}$. Average (red line) and scatter bars (± 1 standard deviation) are overlaid. Winter (summer) changes are solid (dashed) curves. Roughly 40% of ΔVol_{bface} is observed when $h_{trunc} = \text{MSL}$ (vertical dashed line). Circles in (a) indicate $h_{trunc} = h_{bface}$.

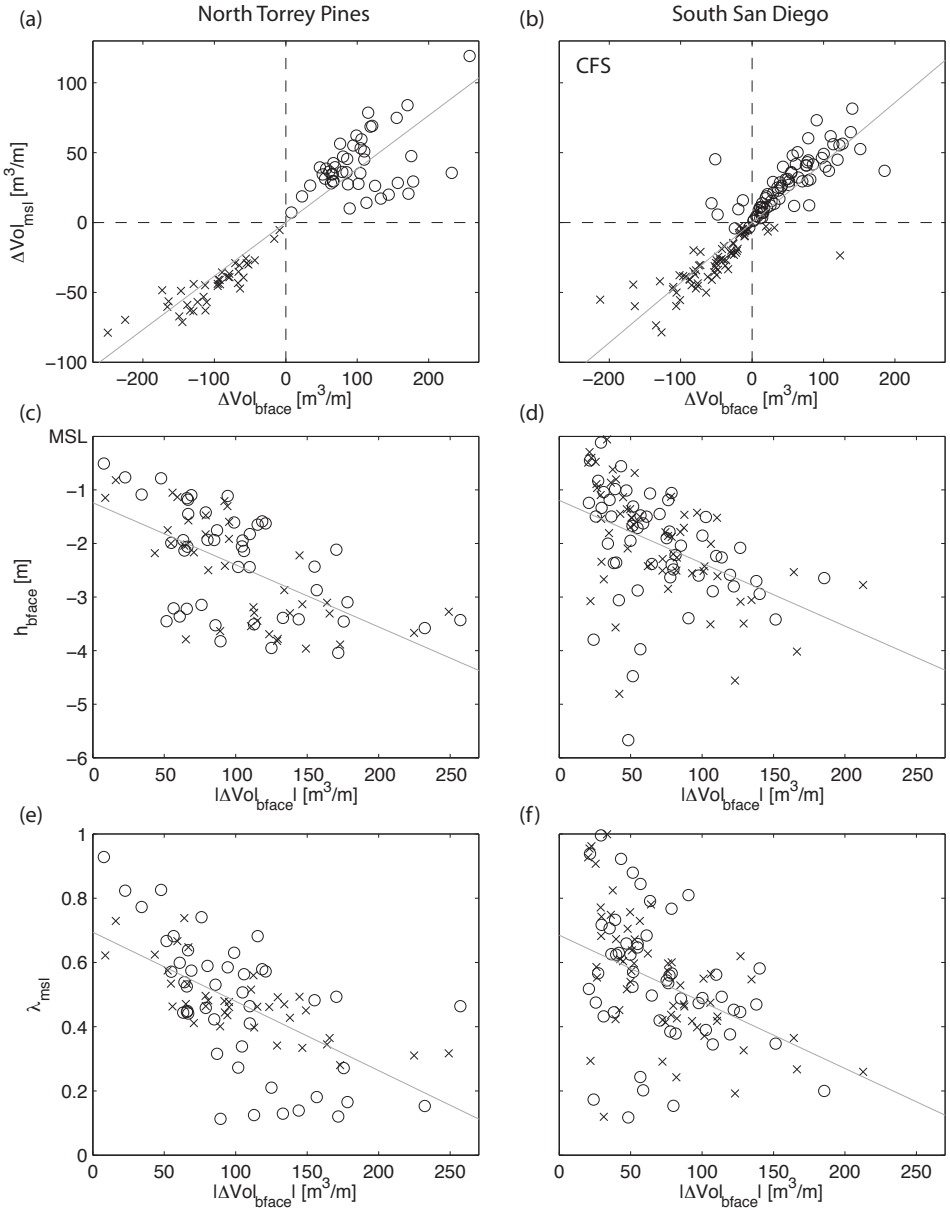

Figure 1.5: North Torrey Pines (left column) and South San Diego (right column) bulk (e.g. many transects) regressions for (a),(b) ΔVol_{MSL} versus ΔVol_{bface}, and (c),(d) h_{bface} and (e),(f) λ_{MSL}, all versus $\left|\Delta Vol_{bface}\right|$. See Table 1.1 for regression statistics. Summer (o) changes and winter (x) changes indicated. The 6 transects included in the bulk South San Diego regressions have significant R^2 when regressed individually for h_{bface} and λ_{MSL}, both versus $\left|\Delta Vol_{bface}\right|$ (Figure 1.6).

right panels in Figure 1.5, and see Table 1.1). In the few surveys where ΔVol_{MSL} and ΔVol_{bface} had opposite sign (Figure 1.5b), volume changes were small and the depth profiles crossed several times.

To illustrate general dependences, multiple transects are combined in the regressions of Figure 1.5. Analysis of individual transects yields $\left|\Delta Vol_{bface}\right|$ to λ_{MSL} regression slopes usually between -0.002 and -0.01 m/m^3, and slopes for $\left|\Delta Vol_{bface}\right|$ to h_{bface} about -0.5×10^{-2} and -4.2×10^{-2} m^2/m^3. A few transects with larger slopes had small volume changes (root-mean-square (RMS) $\Delta Vol_{bface} \le 50\,\mathrm{m}^3/\mathrm{m}$; Figures 1.6a,b; triangles).

1.5 Discussion and summary

Subaerial surveys, often acquired with topographic lidar (airborne and ground-based) or GPS-equipped ground vehicles, are important to beach monitoring. We have compared seasonal volume changes based on the subaerial section of the beach with full depth profiles. The fraction λ_{MSL} of total beach face volume change included in a truncated survey (1.2) depends on the survey termination depth, h_{trunc}, and the depth separating profile changes of opposite sign, h_{bface} (Figure 1.2).

Based on many surveys, winter beach face erosion (and the subsequent summer beach face accretion) extends from the back beach (several meters above MSL) to about -0.5 to -4 m below MSL (Figures 1.5c,d), depending primarily on wave conditions. Wave conditions from any single wave event vary alongshore owing to

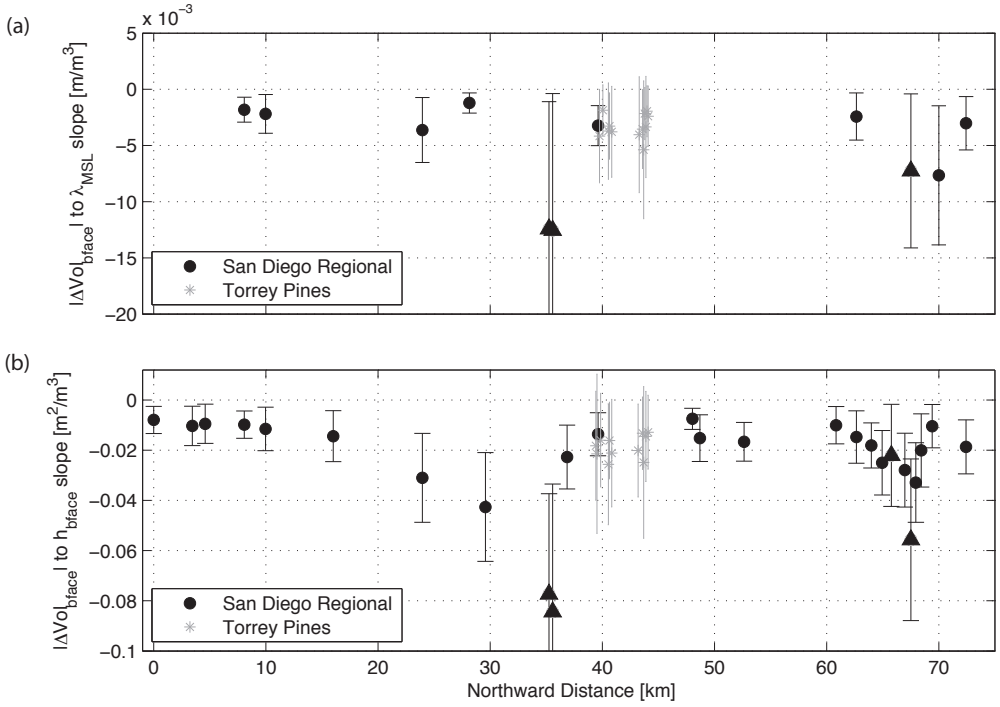

Figure 1.6: Regression slopes with 95% confidence intervals for individual transects (a) λ_{MSL} versus $\left|\Delta Vol_{bface}\right|$ and (b) h_{bface} versus $\left|\Delta Vol_{bface}\right|$, both versus northward distance from southernmost transect. Regression slopes shown are transects with a significant R^2 (Figure 1.1: red markers). Transects with relatively small RMS ΔVol_{bface} ($\leq$ 50 m^3/m) are indicated with triangles. Grey color indicates Torrey Pines. Combined northern Torrey Pines and combined southern San Diego bulk regressions are shown in Figure 1.5.

sheltering by offshore islands; different sections of shoreline are more or less exposed to ocean swell waves arriving from a particular direction. Typically, relatively energetic winter waves heights are in the 2-5 m range, with periods between 6-18 sec. In years with energetic waves, the total erosion is relatively large and extends to deeper water. Typical subaerial surveys are limited to MSL and above; λ_{MSL} varied between about 0.1 and 0.9 (Figures 1.5e,f; Table 1.1).

At some alongshore locations, erosion resistant rock, cobble layers, and limited sediment supply can be seasonally important, restricting upper beach face erosion. Erosion above MSL reaches a geologically determined limit with moderately erosive waves. Further erosion, in severe conditions, occurs in the region below MSL, which is not sampled by subaerial surveys. Such geological features may contribute to the substantial alongshore variation of λ_{MSL} statistics (Figure 1.6).

It does not appear possible to reliably estimate full beach face volume changes from subaerial volume changes at alongshore locations lacking nearby historical full bathymetry transects. Naturally, subaerial surveys of beaches with wave climates, tides, and geological settings different from southern California could behave much differently. The conclusion here is cautionary. The relationship between volume changes from subaerial and full profiles is variable and poorly understood.

Table 1.1: Torrey Pines and San Diego bulk regression slope statistics with 95% confidence limits and R2, and h_{bface} bulk average and standard deviation. R2 > 0.12 are significant at the 95% level. Corresponding regression plots for southern Torrey Pines and northern San Diego are shown in Figure 1.5.

	ΔVol_{bface} to ΔVol_{MSL} $\left(R^2\right)$	$\left\|\Delta Vol_{bface}\right\|$ to h_{bface} $\left(R^2\right)$ (10^{-2} m^2/m^3)	$\left\|\Delta Vol_{bface}\right\|$ to λ_{MSL} $\left(R^2\right)$ (10^{-3} m/m^3)	$\left\langle h_{bface}\right\rangle$ (σ) (m)
S. Torrey Pines	0.58±0.10 (0.93)	-1.2±0.4 (0.20)	-2.9±1.2 (0.17)	-2.3 (1.1)
N. Torrey Pines	0.38±0.09 (0.87)	-1.2±0.4 (0.36)	-2.2±0.7 (0.41)	-2.4 (1.0)
S. San Diego	0.43±0.08 (0.81)	-1.2±0.5 (0.20)	-2.1±1.4 (0.17)	-2.0 (1.0)
N. San Diego	0.21±0.06 (0.62)	-1.2±0.7 (0.19)	-2.3±3.3 (0.07)	-2.5 (0.8)

Acknowledgements

Funding was provided to the Cooperative Coastal Research Team (CCRT) by the U.S. Army Corps of Engineers and the California Department of Boating and Waterways. André Doria was supported by Fellowships from the University of California Regents, NDSEG, and the National Science Foundation (GRFP). Coastal Frontiers Corporation is thanked for assistance using their data sets.

The text of Chapter 1, in full, is a reprint with minor modifications of the paper "Estimating Changes in Near-Shore Bathymetry with Subaerial Surveys," *Journal of Atmospheric and Oceanic Technology*, 30 (9), 2225-2232, doi: 10.1175/JTECH-D-13-00012.1 (Copyright of the American Meteorological Society 2013). The dissertation author was the primary researcher and first author with guidance provided by R.T. Guza.

2

Observations and modeling of San Diego beaches during El Niño

2.1 Abstract

Subaerial sand levels were observed at five southern California beaches for 16 years, including notable El Niños in 1997-98 and 2009-10. An existing, empirical shoreline equilibrium model, driven with wave conditions estimated using a regional buoy network, simulates well the seasonal changes in subaerial beach width (e.g. the cross-shore location of the MSL contour) during non-El Niño years, similar to previous results with a 5-year time series lacking an El Niño winter. The existing model correctly identifies the 1997-98 El Niño winter conditions as more erosive than 2009-10, but overestimates shoreline erosion during both El Niños. The good skill of the existing equilibrium model in typical conditions does not necessarily extend to extreme erosion on these beaches, where a few meter thick sand layer often overlies more resistant layers. The modest over-prediction of the 2009-10 El Niño is reduced

by gradually decreasing the model mobility of highly eroded shorelines (simulating cobbles, kelp wrack, shell hash, or other stabilizing layers). Over prediction during the more severe 1997-98 El Niño is corrected by stopping model erosion when resilient surfaces (identified with aerial imagery) are reached. The trained model provides a computationally simple (e.g. nonlinear first-order differential equation) representation of the observed relationship between incident waves and shoreline change.

2.2 Introduction

Coastal communities and beaches provide abundant ecological, recreational, and socio-economic wealth (Nicholls et al., 2007; Yang et al., 2012; McLachlan and Brown, 2010). Increasing coastal populations (Moore et al., 1999), long-term climate change (Keeling et al., 1995; Rahmstorf et al., 2007), polar ice melt (Dyurgerov and Meier, 2000; Bamber et al., 2009), and sea-level rise (SLR) forecasts of between 0.8-2 m of SLR by 2100 have raised concerns about the long-term (e.g. centuries) fate of beaches, coastal infrastructure, and coastal cliff retreat (Zhang et al., 2004, Pfeffer et al., 2008; Vermeer and Rahmstorf, 2009; Gallien et al., 2011). At shorter time scales, accelerated coastal erosion may be caused by decadal oscillations in the frequency, severity, and tracks of storms (Graham and Diaz, 2001; Allan and Komar, 2006 & 2002; Ruggiero et al., 2010a). California, Oregon, and Washington beaches suffered severe erosion from the intense and frequent storms during the El Niños of 1997-98 and 2009-10 (Revell et al., 2002, 2011; Barnard et al., 2011).

Effectively managing beaches now, and in a future with potentially altered wave climates, requires quantifying the relationship between beach change and waves.

However, testing of shoreline change models on the U.S. West Coast has been limited. Types of shoreline models include process-based and empirical. Process models (e.g. SBEACH, Larson and Kraus, 1989; XBeach, Roelvink et al., 2009; and CSHORE, Johnson et al., 2012) parameterize the complex physics of sediment transport with combined steady and oscillatory flows. Empirical models based on an equilibrium hypothesis tune "bulk response" parameters, and have skill in simulating observations of shoreline change on time scales of months to a few years (Miller and Dean, 2004; Yates et al., 2009a; Davidson et al., 2010, Ruggiero et al., 2010b, Davidson et al., 2013; Splinter et al., 2014). Equilibrium beach models quantify the hypotheses (Wright et al., 1985) that: (a) for a constant wave field, there is an equilibrium beach morphology (the equilibrium beach) that would remain constant in time, neither eroding nor accreting, (b) a beach in disequilibrium with the ambient waves changes toward the equilibrium shape, and (c) the change rate is proportional to the disequilibrium. Miller and Dean (2004) applied equilibrium concepts to derive

$$\frac{dS}{dt} = k(S_{eq}(t) - S(t)) \tag{2.1}$$

where S is the shoreline location (defined as the cross-shore position of a shallow depth contour, here Mean Sea Level (MSL), $S_{eq}(t) - S(t)$ is the beach disequilibrium, and the empirical k depends on wave energy, grain size, and other local factors. Yates et al. (2009a) (hereafter *Y09*) showed that an equilibrium shoreline model had skill at three southern California beaches over five years (2004-2009). Ludka et al. (2015) recently developed an equilibrium beach profile model using up to 10 years of

observations that included the 2010 El Niño. Here, the southern California observations of previous studies (Shepard, 1950, Winant et al., 1975; Nordstrom and Inman, 1975; Flick and Waldorf, 1984, Yates et al., 2009a, 2009b, 2009c) are expanded to include additional sources spanning up to 16 years (1997-2014), including the more severe 1997-98 El Niño winter. The *Y09* shoreline model is extended by gradually decreasing the model mobility of highly eroded shorelines (coarsely accounting for cobbles and other natural armoring), and stopping erosion when a non-erodible layer (e.g. bedrock) is reached.

In this chapter, the beach sites (Section 2.3) and wave and sand level observations (Section 2.4) are described. In Section 2.5, observations of waves and shoreline (MSL contour) location are used to tune an equilibrium-type shoreline model. Results are discussed in Section 2.6, and summarized in Section 2.7.

2.3 Beach sites

In Southern California, wave conditions and beach sand levels vary seasonally (Shepard, 1950, Winant et al., 1975; Nordstrom and Inman, 1975; Flick and Waldorf, 1984, Yates et al., 2009a, 2009b, 2009c). Sand elevations were measured at five San Diego County beaches (from south to north, Figure 2.1): Imperial Beach (4 km alongshore span), Torrey Pines (8 km), Solana Beach (2.6 km), Cardiff (2 km), and Camp Pendleton (2.5 km). Median sand sizes range between 0.15-0.28 mm (Table 2.1), and beach slope between 0.01-0.08 m/m (Table 2.1).

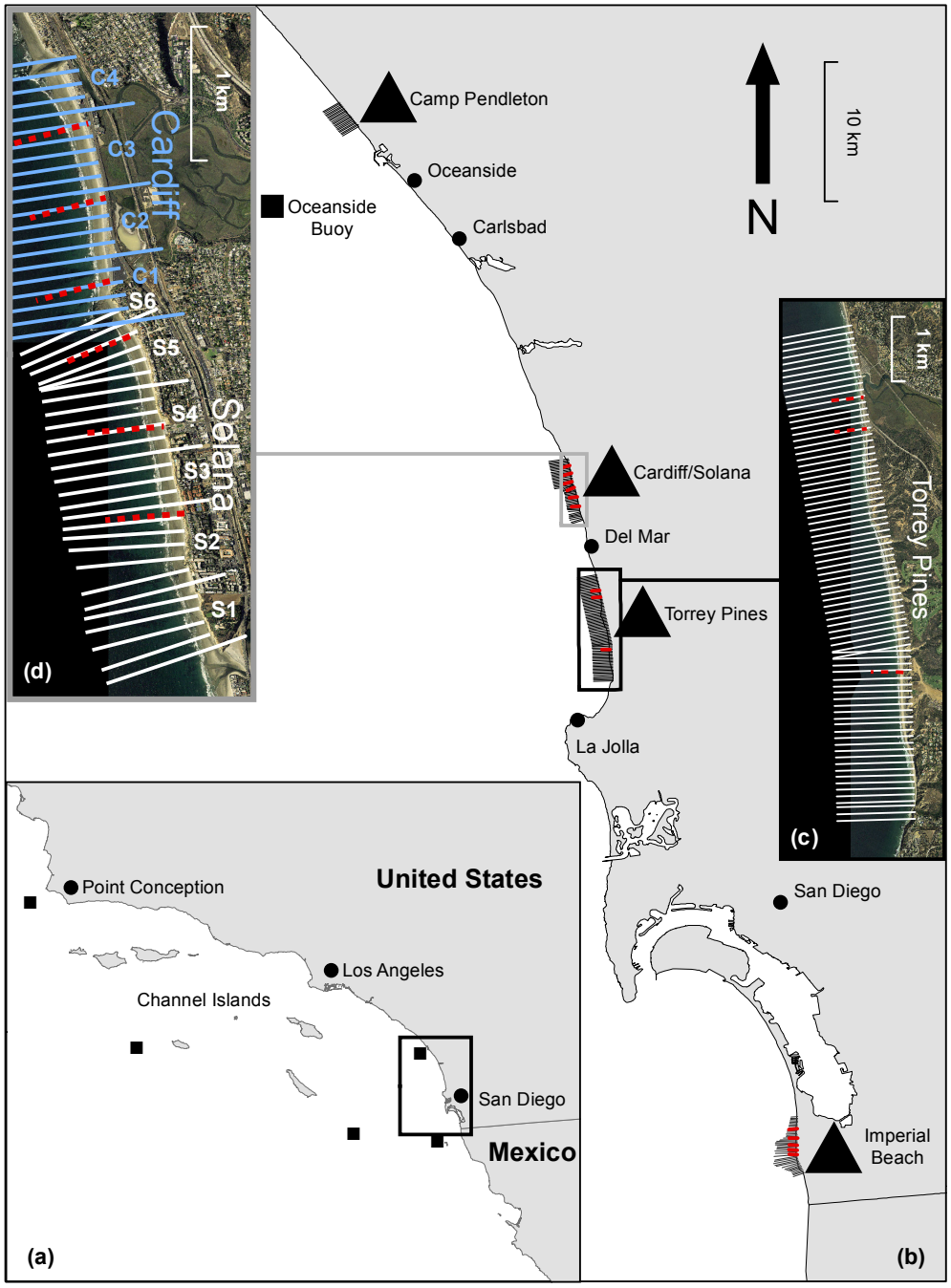

Figure 2.1: (a) Southern California map with wave buoy locations (black squares). (b) San Diego area map with study beaches (black triangles), near-shore buoy (black square), and survey transects (black (red) lines are SIO (SANDAG) transects). (c) Torrey Pines and (d) Solana Beach and Cardiff plan views. Cross-shore transects of SIO quarterly surveys (January, April, July, October) are white and blue lines, and SANDAG biannual (May, October) are red lines. For model comparisons, surveys were alongshore averaged in 500 m segments, labeled in (d).

Table 2.1: Beach alongshore distance, beach facing azimuthal direction, median sand grain diameter (D_{50}), beach slope at MSL, MSL minimum, maximum, and standard deviation horizontal displacement from average MSL location, number of surveys, and survey date range for each site.

Site	Alongshore Distance (km)	Direction (deg)	D_{50} (mm)	Beach Slope	MSL min/max (σ) (m)	Number of Surveys	Date Range
Imperial Beach	4	250-270	0.28[a]	0.02-0.05	-23.6/25.8 (10.5)	97	Oct 1997-Aug 2012
Torrey Pines	8	260-270	0.15[b]	0.01-0.08	-31.5/26.2 (9.1)	226	Oct 1997-Jan 2014
Solana Beach	2.6	240-265	0.15[b]	0.02-0.08	-22.5/20.5 (7.6)	103	Oct 1997-Aug 2012
Cardiff	2	260	0.15[b]	0.02-0.11	-27.3/22.8 (9.5)	136	Oct 1997-Aug 2012
Camp Pendleton	2.5	235	0.18[b]	0.02-0.04	-35.8/19.4 (9.7)	72	Oct 1998-Oct 2010

[a]Collected May 2008 in the swash zone (Warrick et al., 2012).
[b]Collected spring 2006 near the high tide line (Yates et al., 2009b).

Imperial Beach (Figure 2.1b) contains a recreational pier, two short groins in the northern 700 m, and the Tijuana River mouth at the southern end. Most of the beach is backed by low-lying urban development and protective riprap, seawalls, and cobble berms (Figure 2.2). The southern 6.5 km of Torrey Pines State Beach (Figure 2.1c), is backed by 50-110 m high-relief sandstone cliffs, and the northern 1.5 km is fringed by riprap and the Los Peñasquitos Lagoon inlet (Moore et al., 1999; Young et al., 2010). Solana Beach (Figure 2.1d) is backed by 25-m sandstone cliffs (Young et al., 2010) often armored with seawalls and gunite. Cardiff (Figure 2.1d) is a straight, narrow beach that extends 2 km north from Solana Beach to the San Elijo Lagoon inlet. Riprap and public parking lots border the back beach. A 200-m long cobble berm, near the upper swash limit, is located at the southern end of the Cardiff site. The Camp Pendleton site (Figure 2.1b) spans 2.5 km north from the Santa Margarita River outlet, and the beach is backed by a vegetated low dune. During energetic winters, foreshore cobble patches (10s of meters in lateral extent) can be exposed at all beaches except Camp Pendleton, which is sandy year-round.

Digital orthographic and non-orthographic imagery was used to characterize the back beach type (e.g. seawall, hard cliff, soft dune, rip-rap, none) and the exposed beach face substrates (e.g. bedrock, cobbles, mixed, unknown) during the El Niño 2010 winter (Figure 2.2). The non-orthographic aerial imagery (Figure 2.2b) was collected near the 2010 El Niño maximum erosion (e.g. February 1-2, 2010) during low tide from a U.S. Coast Guard (USGS) helicopter with a high-resolution digital

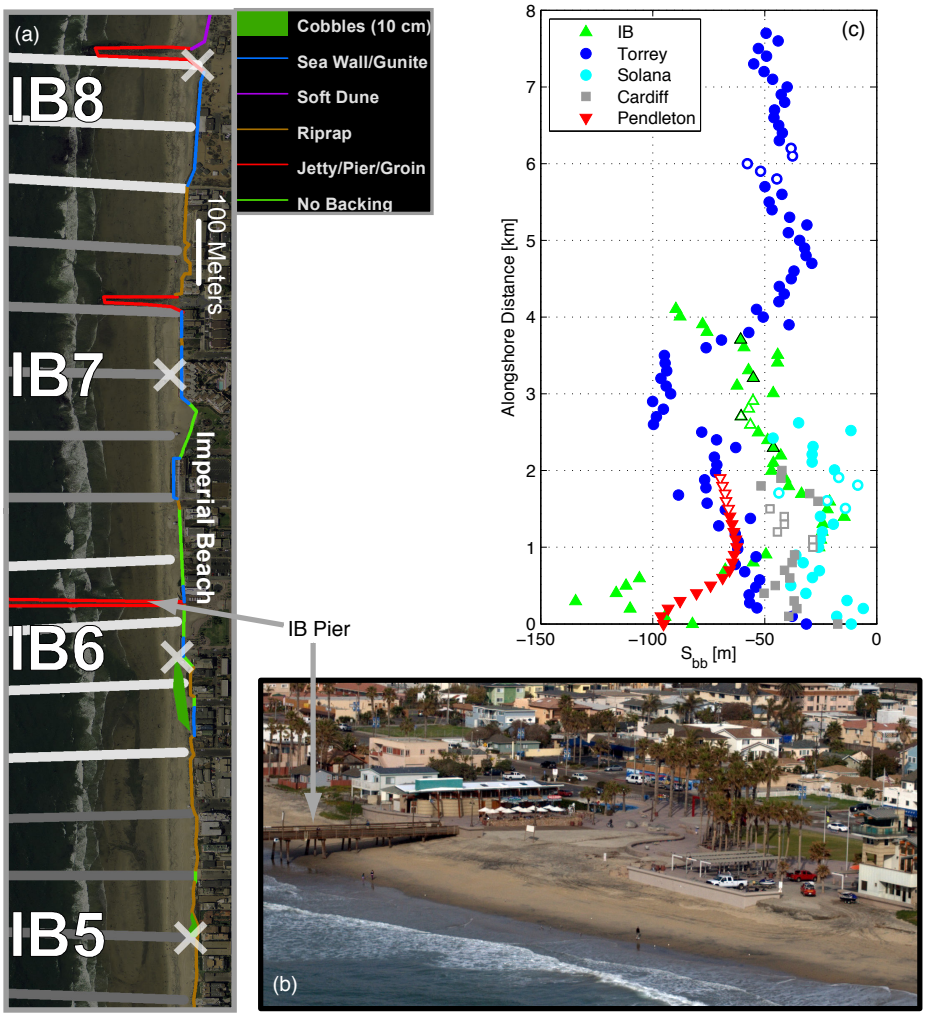

Figure 2.2: (a) Aerial image of Imperial Beach with subaerial substrate and back beach types (legend). Cross-shore survey transects, spaced 100 m alongshore, are averaged over approximately 500 m alongshore sections for modeling (IB5-IB8; (a) centers marked with white crosses). Transects within model section are indicated by alternating white and gray transect shadowing (end sections have additional transects outside of frame (a)). (b) Helicopter-based image of Imperial Beach (section IB6; February 2010). Imperial Beach Pier in (a) and (b) is indicated with gray arrows. (c) The non-erodible shoreward boundary cross-shore location S_{bb} (referenced to the average shoreline (MSL) location; negative is shoreward) on each transect versus alongshore distance for all five beaches. $S_{bb} \approx$ -58 m for the heavily cobbled backbeach in section IB6 (alongshore distance 2.6-2.9 km). Location of 500 m modeled sections, for each beach in Figure 2.6, are indicated by markers with white centers in (c), and black edged triangles in (c) correspond to locations of transects nearest to white crosses in (a).

single-lens reflex (DSLR) camera. Orthographic aerial imagery was collected by Fugro EarthData, Inc. from 26 August to 29 November, 2010 using an airborne orthographic imaging system (Leica ADS40-SH52) with 2-m horizontal accuracy and 30-cm pixel resolution.

The non-orthographic 2010 winter aerial imagery was visually referenced to the orthographic imagery to estimate the horizontal locations of subaerial beach substrates exposed during El Niño 2010 erosion (colored polygons in Figure 2.2a). Non-erodible surfaces above the sand level included boulders, rock outcroppings and ledges, cobble berms and low relief bedrock. Features visible in 2010 above MSL (e.g. the cobbles in Figure 2.2b are above MSL) were assumed to continue below sand level at the same steep slope. Low relief features exposed in 1997-98 may not have been detected in 2009-10.

The vertical elevations of exposed non-erodible surfaces were then estimated from the airborne lidar survey (February 26, 2010) occurring 24 days after the USGC aerial photo survey. Lidar and imagery-based estimates of the subaerial substrate locations and types agreed qualitatively with subaerial all-terrain vehicle (ATV) substrate surveys collected at all sites within 9 days of the aerial photo survey. Comparable detailed mapping was not available for the 1997-98 El Niño.

2.4 Observations

2.4.1 Sand Level Surveys

Surveys of subaerial beach sand levels from 1997-2014 at 5 beaches were obtained from several sources (Figure 2.1) including (1) biannual cross-shore transects

extending from the back beach to ~8-10 m depth beginning in 1997 (San Diego Association of Governments (SANDAG); red transects in Figure 2.1) and (2) quarterly cross-shore transects, beginning in 2004 (SIO; dense black, blue, or white transects in Figure 2.1) (*Y09*). (3) Monthly subaerial shoreline parallel surveys beginning at Torrey Pines, and subsequently expanded to four additional sites (Imperial, Cardiff, Solana, and Camp Pendleton). (4) Airborne lidar in April 1998 (NASA's airborne topographic mapper (ATM); Brock et al., (2002)) and biannually from May 2002 until October 2010 (Univ. of Texas, Yates et al., (2008)). Lidar returns were removed offshore of the waterline location, estimated using water levels from a nearby tide gauge and runup approximated using local wave conditions (Yates et al., 2008). Lidar sand levels were gridded onto 4 m^2 cells, using the cell median elevation to reduce the influence of outliers. Point density in the 1998 NASA lidar survey was low (0.57 points m^{-2}), compared with the post-2001 biannual lidar surveys (~2 points m^{-2}) (Brock et al., 2002; Yates et al., 2008). Grid cells with less than 3 data points were discarded from the post-2001 lidar surveys. All data were necessarily retained in the lower density 1998 survey. Surveys from different sources at the same approximate time and beach usually agree, with differences owing to variable amounts of spatial averaging (Figure 2.3).

Responding to seasonal variations in wave energy, the observed shoreline (e.g. MSL contour) locations usually varied seasonally by 25-30 m at all 5 study beaches (Figure 2.4; Winant et al., 1975; Yates et al., 2009b). During the 1998 El Niño, shoreline retreat was maximal, about 25 m landward of the typical (e.g. 2004-2012)

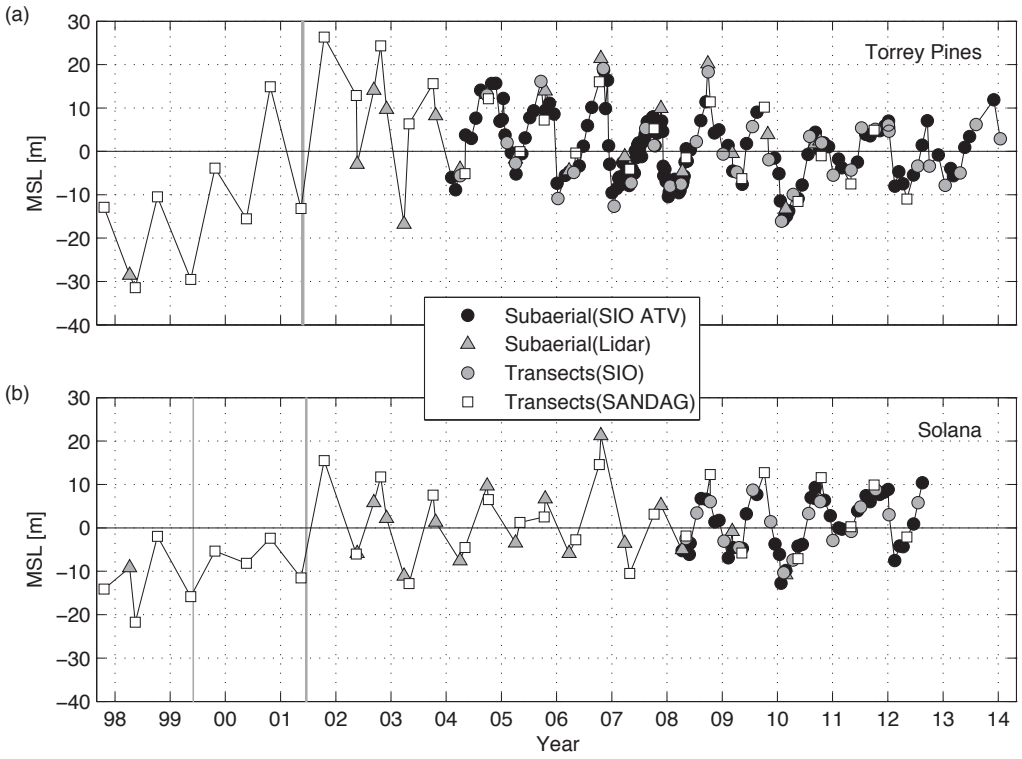

Figure 2.3: MSL cross-shore position (demeaned and alongshore averaged) versus time (tics are 1 January) for 16 years at (a) Torrey Pines and (b) Solana Beach. All available transects of each survey (legend indicates survey type, see Figure 2.1) are averaged. Positive (negative) values correspond to a wide (narrow) subaerial beach. Vertical gray lines indicate beach nourishment periods.

winter shoreline (Figure 2.4). Recovery from 1997-98 took several years, even with nourishments both shortly before (1997, Imperial Beach, 178,000 m^3) and after (1999, Solana Beach, 41,000 m^3) El Niño; however, during fall 1997, existing beach sand levels at several sites were historically lower than post-summer levels observed in most other years. Accordingly, the erosive change during the 1997-98 El Niño was limited because of low sand levels preceding the event. Recovery following the less erosive 2009-10 El Niño was more rapid, effectively one season (Figures 2.3 and 2.4). Spring-summer 2001 nourishments at Imperial Beach, Torrey Pines, Solana Beach,

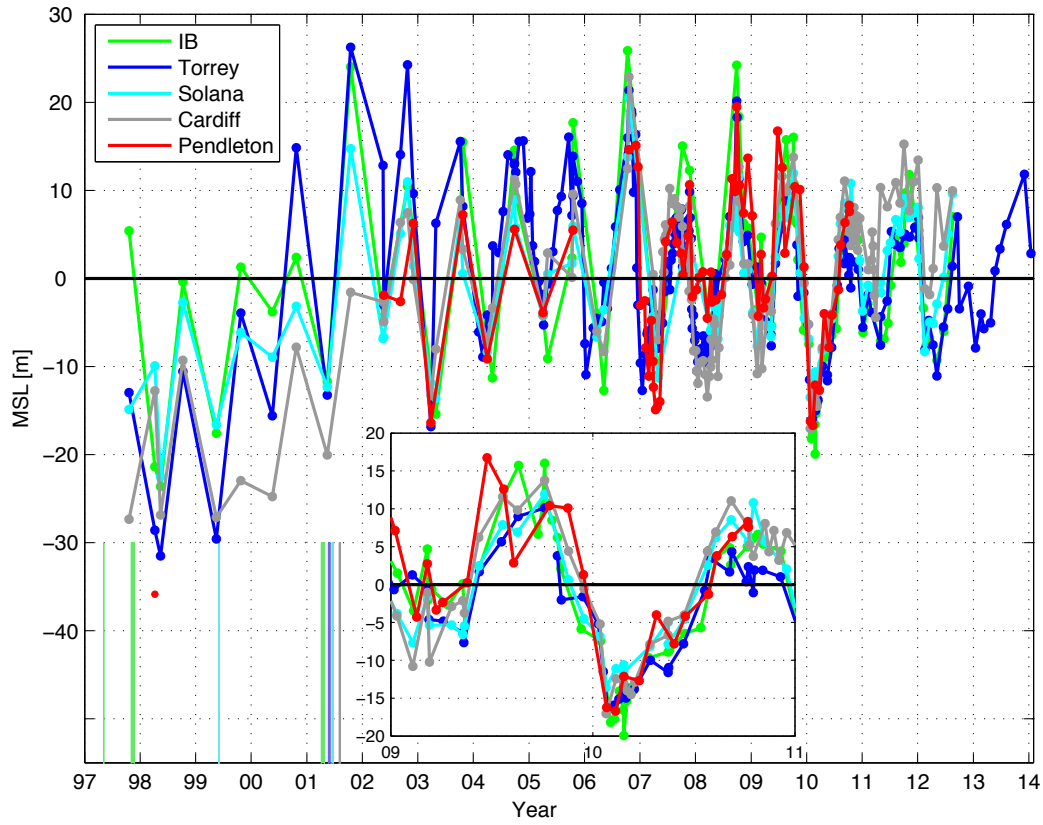

Figure 2.4: MSL cross-shore position (demeaned and alongshore averaged) versus time (tics are 1 January) for 16 years at 5 sites (see legend) from all data sources. Shortened colored vertical lines (see legend) indicate beach nourishment periods (see Table 2.2). Inset expands the 2009-10 El Niño winter.

and Cardiff elevated sand levels to new maxima (Figure 2.4). The nourishment was detectable for about two years at Torrey Pines, either as a wider subaerial beach, or as an enhanced offshore winter sand bar (Yates et al., 2009c). SANDAG winter surveys occur in spring and fall. The spring surveys usually occur after the winter erosion maximum in February-March (compare squares and circles in Figure 2.3a, in 2005-2008 inclusive), so the 1998 survey may not have captured the maximum erosion.

Table 2.2: Historical beach nourishment placement dates, receiver sites, qualitative placement locations, nourishment volumes, nourishment pad approximate length and width, and nourishment sand median grain diameter (D_{50}).

Placement Date	Receiver Site	Placement Location	Volume (10^3 m^3)	Length (m)	Width (m)	D_{50} (mm)
1995	Imperial Beach	Near-shore[a]	31.3	-	-	-
1996	Imperial Beach	Near-shore[a]	35.9	-	-	-
1997	Imperial Beach	Subaerial Beach[b]	13.7	-	-	-
1997	Imperial Beach	Near-shore[a]	178.1	-	-	-
1999	Solana Beach	Subaerial Beach	41.2	-	-	-
6-27 April, 2001	Torrey Pines	Subaerial Beach	187.3	488	49	0.14
22 May-4 June, 2001	Imperial Beach	Subaerial Beach	91.7	701	37	0.24-0.52
15-24 June, 2001	Solana Beach	Subaerial Beach	111.6	579	21	0.14
2-10 August, 2001	Cardiff	Subaerial Beach	77.2	274	46	0.34

[a]Placed in near-shore depths beneath the water surface.
[b]Placed south of the Tijuana River Mouth.
(Coastal Frontiers Corporation, 2002; California Department of Boating and Waterways and State Coastal Conservancy, 2002)

2.4.2 Waves

Waves typically approach the Southern California Bight from north-northwest in winter and from south-southwest in summer and vary alongshore owing to sheltering by the Channel Islands and refraction over complex offshore bathymetry (Pawka, 1983). Local (e.g. < 30 m depth) bathymetric variations further refract and focus waves with appreciable alongshore energy variations over several hundred meters alongshore. Directional wave buoys (CDIP, http://cdip.ucsd.edu; Figure 2.1a) initialized a spectral refraction model (O'Reilly and Guza, 1991, 1993, 1998) that provided hourly wave estimates at 10 m depth every 100 m alongshore. Near-shore buoy deployments confirmed reasonably good model accuracy in relatively shallow water (20-30 m depth) at several of the study sites (Young et al., 2012).

Waves were most energetic during strong El Niño winters (Figure 2.5a). For example, at the Oceanside buoy (Figure 2.1b), the hours of significant wave height H_s exceeding 3 m were between 0-26 hours during 13 non-El Niño winters, compared with 40 and 51 hours in the 1997-98 and 2009-10 El Niño winters, respectively. Total hours of H_s between 2-3 m during the 1997-98 El Niño winter (more than 400 hours) dwarfed all other winters, nearly doubling those found in the second most energetic winter (e.g. 2009-10 winter; 220 hours of H_s = 2-3 m; Figure 2.5a). In 1997-98, H_s exceeded 2 m for nearly 60 continuous hours, with frequent and prolonged sequences of energetic waves in early December 1997 and February 1998 (Figure 2.5b). January 2010 had the longest period (~140 hours) of continuous H_s exceeding 2 m (Figure 2.5e).

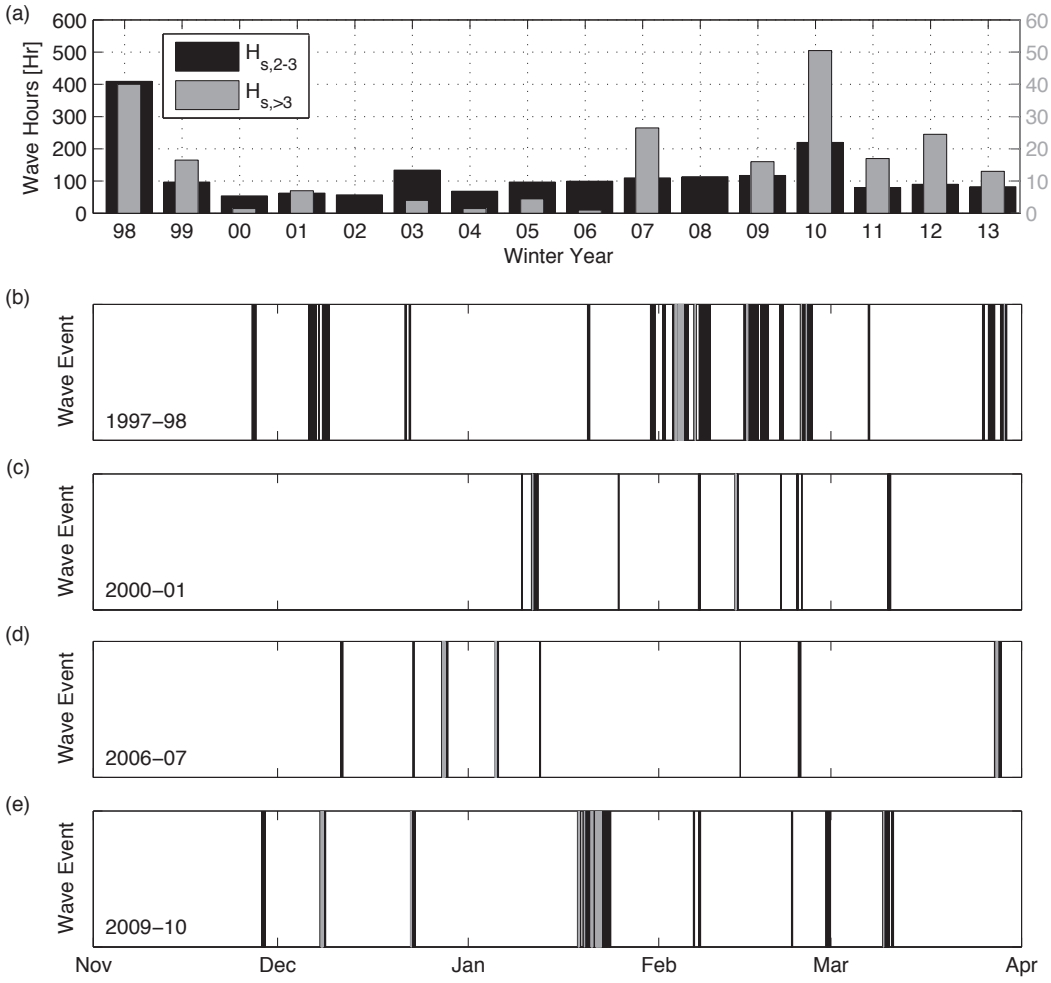

Figure 2.5: (a) Hours of observed H_s between 2-3 m, and greater than 3 m (see legend) versus winter year (November-March) from November 1997 through March 2013 at Oceanside Buoy (Figure 2.1). Temporal occurrences of wave events within H_s ranges (legend) for winters (b) 1997-98 (El Niño), (c) 2000-01, (d) 2006-07, and (e) 2009-10 (El Niño).

2.5 Shoreline Modeling

2.5.1 Equilibrium shoreline model

An existing equilibrium shoreline model (*Y09*) was modified to improve predictions during El Niños and other severe erosion conditions by accounting for

durable limits (e.g. bedrock, seawalls, hard cliffs). We assume these relatively resilient boundaries were not eroded during the modeling period, and neglect cliff erosion, which would both relocate the back beach boundary and supply new sand to the beach. The differences in beach profiles with armored and exposed back beaches are not included. Tides (~2 m spring range) are excluded from the shoreline change model for simplicity. Most storms last at least one tidal cycle, so the depth at the cross-shore location of the MSL contour (used as a generic shoreline) varies from about 1 m to exposed. Validation of a model that includes the effect of tide levels would require sand level change observations that resolve change within a tidal cycle, whereas all of the present observations are at low tide. With the shoreline location S defined as the cross-shore location of the MSL contour, the shoreline change rate dS/dt depends on the present shoreline position S and incident wave energy E,

$$\frac{dS}{dt} = \begin{cases} C^{\pm} E^{1/2} \Delta E(S) & \text{for } S > S_{bb} \\ 0 & \text{for } S \le S_{bb} \end{cases} , \qquad (2.2a)$$

where $C^{\pm}$ are two change rate coefficients for accretion (C^{+}) and erosion (C^{-}), and the wave energy disequilibrium is

$$\Delta E(S) = E - E_{eq}(S) . \qquad (2.2b)$$

E_{eq}, the equilibrium wave energy, is the wave energy for a given S that would cause no shoreline change. For the few occasions when highly accreted shoreline positions S^{+} yielded non-physical negative equilibrium wave energy E_{eq} (e.g. $E_{eq}(S^{+}) < 0$),

$E_{eq}(S^{+}) \equiv 0$, ensuring non-negative equilibrium wave energy. Unless otherwise noted, E_{eq} is linearly related to the shoreline position S:

$$E_{eq}(S) = a_0 + a_1 S, \tag{2.3}$$

where a_0 and a_1 are empirically determined coefficients. New here (2.2a), S_{bb} is the non-erodible back beach cross-shore location defined using the aerial photographic and lidar surveys. Shoreline retreat stops (e.g. $dS/dt = 0$) when $S = S_{bb}$. A beach initially in equilibrium and subject to a step change in the incident wave energy equilibrates exponentially, with a characteristic e-folding time scale $\tau^{\pm} = \left| a_1 C^{\pm} \sqrt{E} \right|^{-1}$ (*Y09*).

Each beach was sub-divided into approximately 500 m alongshore sections, numbered from south to north within each site: I1-I9 (Imperial Beach), T1-T9 (Torrey Pines), S1-S5 (Solana Beach), C1-C4 (Cardiff), P1-P4 (Camp Pendleton). Incident wave energy, temporally-demeaned shoreline observations, and the back beach limit S_{bb} (Figure 2.2) were alongshore averaged on transects within each 500 m section. Values of the model's four free parameter (C^{+}, C^{-}, a_0, a_1) were determined from these averaged shoreline observations and hourly wave estimates by minimizing the model-data root-mean-square error (RMSE) using surrogate management framework (SMF) optimization (Booker et al., 1999; Marsden et al., 2004)

2.5.2 Model-data comparison

Shorelines were hindcast for up to 16 years using the wave-driven equilibrium model, initialized with the earliest survey data point (typically fall 1997). Model

calibration with a period including an El Niño yielded improved model-data agreement during both El Niño and non-El Niño years, and calibration with 2003-2011 data is shown (Figure 2.6). The average model skill (R^2), where R^2 is defined as $\left(\frac{\langle xy \rangle}{\sigma_x \sigma_y}\right)^2$, at Solana, Imperial and Torrey Pines beaches are between 0.55-0.60 (Table 2.3). At Cardiff and Camp Pendleton, two shorter beaches with river or lagoon mouths, R^2 was often less than 0.5. Two of the four modeled sections at Cardiff have low R^2 (e.g. 0.22 and 0.41) and are located near a persistent lagoon mouth or a large bedrock platform extending from the subearial beach to wading depths. Camp Pendleton was observed for the shortest time, and has the lowest R^2 (less than 0.5 at all modeled sections; Figure 2.6e), possibly resulting from the adjacent river mouth. Skill at all modeled locations was significant at the 95% level.

The model back beach erosive limit S_{bb} (Figure 2; dashed horizontal line in Figure 6a-d) was reached during the 1997-98 El Niño (except at Camp Pendleton), and without the geological constraint the unmodified Y09 model over-predicted erosion (red curve in Figure 6). S_{bb} was reached only at a few sites during the 2009-10 El Niño. The maximum model beach width $S_{\max} = -a_0/a_1$ (positive horizontal dotted line in Figure 6) was exceeded a few times, usually after sand nourishments that are neglected in the model (e.g. accretion peaks in fall 1998 and fall 2001 at Imperial Beach (Figure 6a) and during summer-fall 2001 at Torrey Pines and Solana Beach (Figure 6b,c). The anomalous accretive peak in summer 2006 at many of the sites is unexplained and not reproduced by the model.

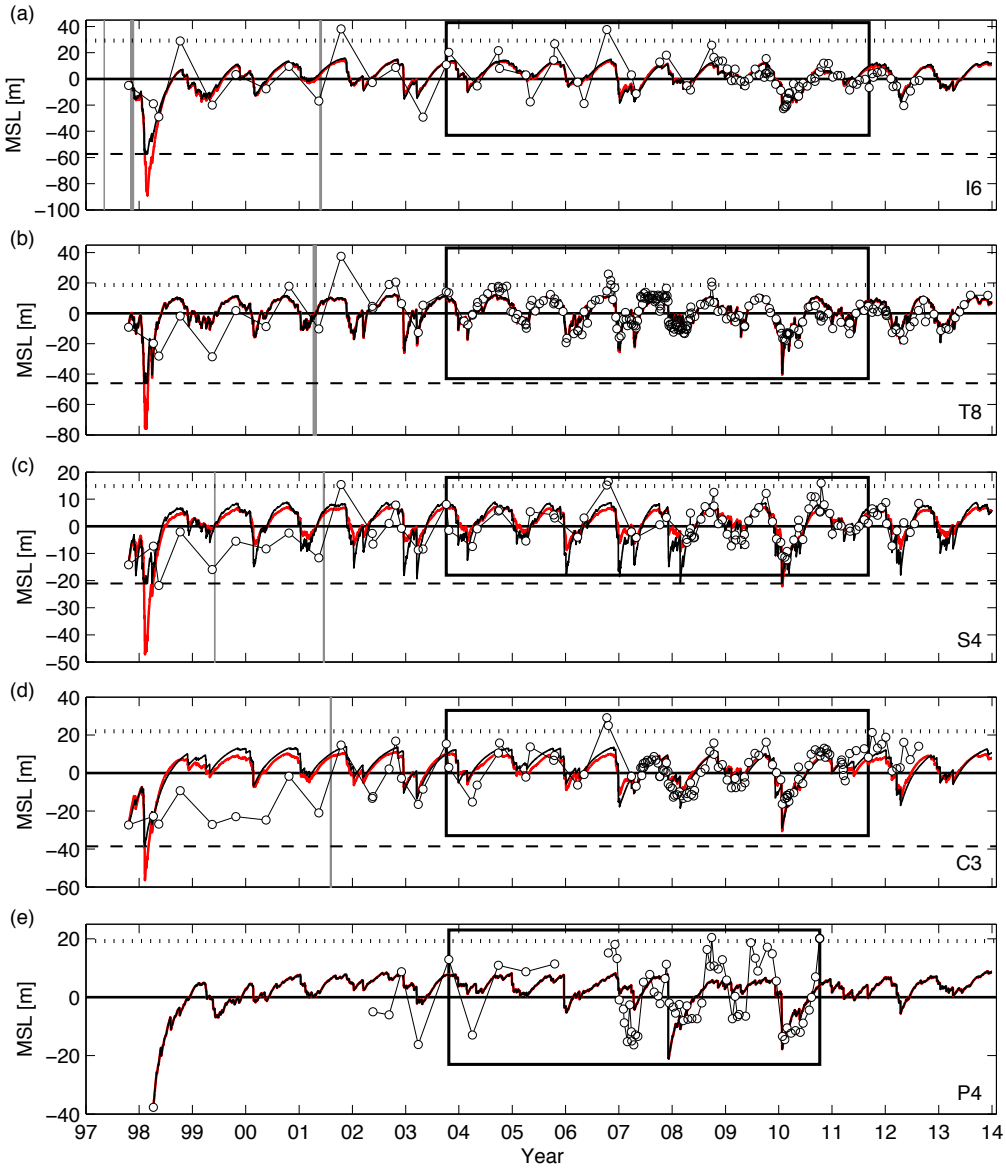

Figure 2.6: MSL position versus time (tics are 1 January) for representative 500 m long sections at (a) Imperial Beach (section I6) and (b) Torrey Pines (T8), (c) Solana Beach (S4), (d) Cardiff (C3), and (e) Camp Pendleton (P4). Shoreline observations are white circles. Model predictions (linear$_4$ model, black curve; *Y09* model, red curve) differ primarily in 1997-98. Model calibration period (black rectangle), non-erodible back beach limit S_{bb} (dashed horizontal black line), fully equilibrated shoreline $S = -a_0/a_1$ for $E = 0$ (dotted horizontal black line), and beach nourishments (vertical gray bands) are shown. Model root-mean-square errors (R^2) over 16-years are (a) 8.6 m (0.57), (b) 6.3 m (0.65), (c) 5.2 m (0.52), (d) 8.9 m (0.41), and (e) 8.8 m (0.43).

Table 2.3: Alongshore averages and standard deviations of optimal model free parameters and R^2 at each site. Average characteristic adjustment timescales[a] $\tau^{\pm}$ are shown in parenthesis and have units of days. The calibration period is October 2003-October 2011. R^2 is for model runs over all available data.

	a_1 $(10^{-3}\,\mathrm{m^2/m})$	C^- $(\mathrm{mh^{-1}/m^3})$	C^+ $(\mathrm{mh^{-1}/m^3})$	a_1C^- (τ^-) $(10^{-3}\,\mathrm{m^{-1}h^{-1}})$	a_1C^+ (τ^+) $(10^{-3}\,\mathrm{m^{-1}h^{-1}})$	R^2
Imperial Beach	-4.5±1.7	-0.92±0.72	-1.06±0.94	3.5±2.5 (21)	3.6±2.4 (64)	0.55±0.13
Torrey Pines	-2.2±0.9	-3.90±2.67	-4.58±2.02	6.6±3.2 (9)	10.3±5.7 (29)	0.58±0.08
Solana Beach	-5.8±2.5	-1.26±0.67	-0.83±0.43	7.6±3.5 (21)	4.0±1.7 (54)	0.60±0.08
Cardiff	-5.4±3.1	-2.16±1.52	-1.49±1.92	14.3±16.9 (14)	4.7±4.1 (57)	0.43±0.15
Camp Pendleton	-5.9±2.3	-0.62±0.10	-0.79±0.13	3.5±0.8 (12)	4.8±2.5 (41)	0.38±0.03

[a] $H_s = 4$ m (1 m) was used for estimating τ^- (τ^+).

2.6 Discussion

2.6.1 Parameter values, response times, and initialization

Optimal model free parameters varied within and between sites (Table 2.3). Model error is weakly sensitive to the free parameter values, with only a 10% increase in model error for factor of two of changes in parameters (comparable to the differences between sites). Free parameter values likely depend on sediment availability, grain size, and possibly other environmental factors, but are only loosely constrained by the observations.

The best-fit shoreline adjustment time scales $\tau^{\pm} = \left| a_1 C^{\pm} \sqrt{E} \right|^{-1}$, averaged over each site, varied between roughly 10-20 days for erosion τ^{-} (with $H_s = 4$ m), and the accretion τ^{+} spanned 29-64 days (with $H_s = 1$ m; Table 2.3). Hypothetical initial conditions illustrate the rapid return (weeks to several months) of the model to equilibrium from artificially large disequilibria (crosses and triangular markers in Figure 2.7). Six rather different initial conditions in 1996, 1997, and 1998 all result in the same modeled shoreline by summer 1998 (gray curve in Figure 2.7). Model shorelines recovered from the strong 1997-98 El Niño erosion by the next winter, more rapid than the observed multi-year recovery, demonstrating the model's failure to properly reproduce the slow return of sand evidently displaced further offshore during the strong event (Figures 2.6b-d). Accretion is crudely parameterized in the model and requires future study.

2.6.2 Calibration period

At Torrey Pines, *Y09* found model-data RMSE increased 1.9 m in predictive model periods, compared to the calibration period RMSE. Splinter et al. (2013) provide a more extensive calibration and validation discussion of a similar equilibrium-based 1-D shoreline model. Both Y09 and Splinter et al. (2013) showed that approximately two years of monthly observations suffice to calibrate empirical shoreline model parameters on seasonally variable beaches (Torrey Pines in southern California and along the eastern Australian coast). Here, three calibration periods are examined (Figure 2.8): 1997-2013 (all data; 16 years), 2003-2011 (8 years), and 2003-

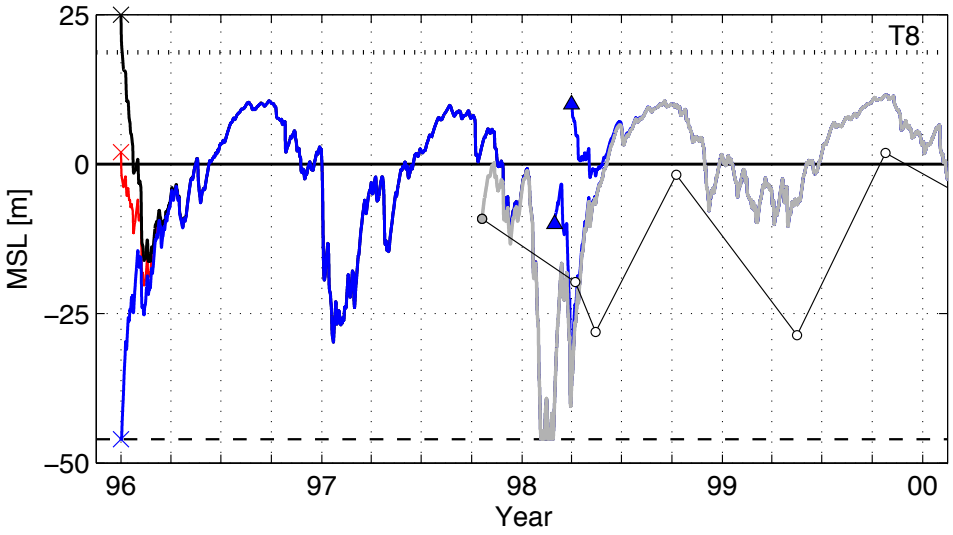

Figure 2.7: Modeled MSL position versus time at Torrey Pines (section T8, calibrated with 2003-2011 data) with different initial conditions. January 1996 with three hypothetical MSL shorelines (~0, 25 and -50 m; colored crosses) yield colored curves that rapidly converge together. Fall 1997 was initialized with the observed shoreline (gray circle and curve) and spring 1998 was initialized with ±10 m (two black-blue triangles). By summer 1998, all 6 model initializations yield the same result (gray curve). Horizontal lines are non-erodible back beach S_{bb} (dashed) and fully accreted beach (dotted), $S = -a_0/a_1$.

2008 (5 years). The 2003-2008 period lacks an El Niño. Model errors are characterized with the RMSE over 16 years, and with Δ_{W10}, defined to be the difference between the maximum erosion observed and modeled during the 2009-10 El Niño winter. Solana Beach results weakly depended on calibration period (Figure 2.8, top). At the other sites, longer calibration periods that included an El Niño

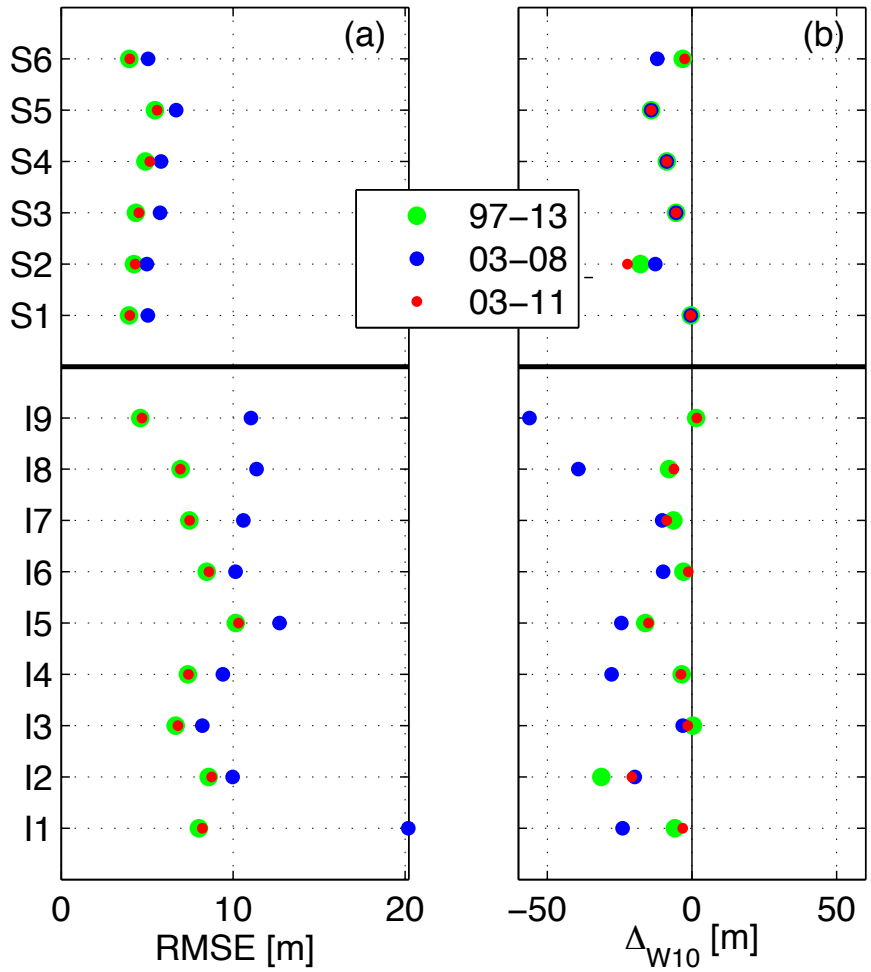

Figure 2.8: Model (linear$_4$) (a) RMSE (all data) and (b) model-data winter (January-March) 2010 erosion minimum error versus each 500 m alongshore section at Solana Beach (top, sections S1-S6) and Imperial Beach (bottom, I1-I9) for three model calibration periods. (b) Negative values indicate model over-predicts erosion minimum.

consistently decreased Δ_{W10} and RSME over the entire 16-year observation period, which included years of neutral and La Niña conditions (Figure 2.9a,b). The sparse 1997-2001 data were not well fit, even when 1997-2001 was included in the calibration (not shown). The 2003-2011 calibration period was used.

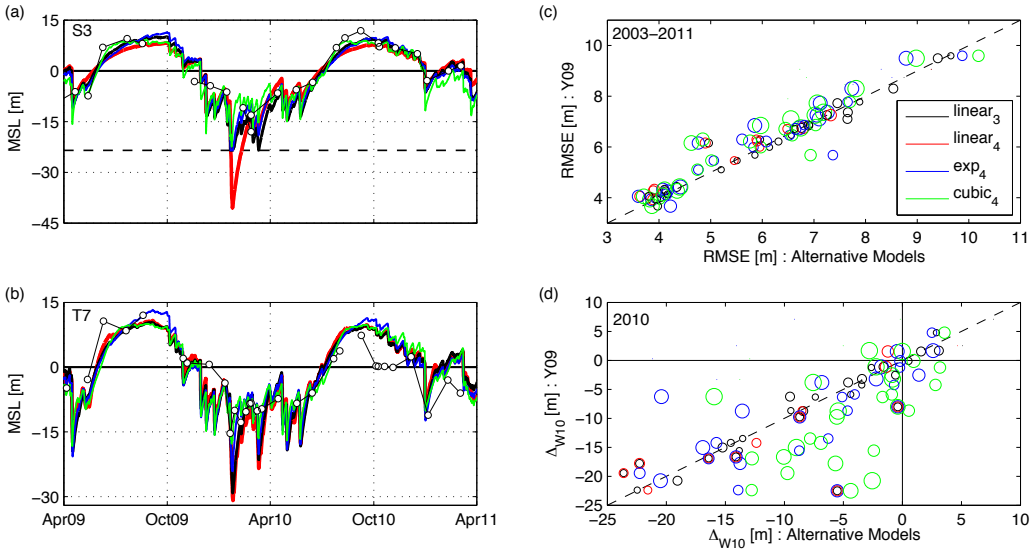

Figure 2.9: Modeled and observed (white circles) MSL versus time at (a) Solana Beach (section S3) and (b) Torrey Pines (T7). (a) Dashed black horizontal line indicates S_{bb}, the non-erodible back beach limit. Red curve in (a) and (b) is the *Y09* (unrestricted linear$_4$) model. Note vertical scales differ in (a) and (b). (c) RMSE (October 2003-October 2011) and (d) model-data winter 2010 (January-March 2010) erosion minimum error for the *Y09* model (vertical axis) versus alternative models. In panels (c) and (d), symbol size varies for visibility. (a-d) Model types are indicated by colors (legend in (c)).

The alongshore variability of the 8-year calibration model coefficients was qualitatively similar to previous work (*Y09*) based on ~5 years of calibration that did not include an El Niño (similar to the 2003-2008 calibration results in this study). Here, the relative magnitudes of the wave energy slope, a_1, and $C^{\pm}$ were reversed

compared to *Y09* (e.g. *Y09* had larger magnitude a_1 and smaller magnitude $C^{\pm}$ compared to this study). These differences may be partially attributed to different calibration periods, and different alongshore spans, here and in *Y09*. More fundamentally, the parameters are not strongly constrained by the observations. For example, the multiplication of model terms (2) allows changes in a_1 to compensate for changes in $C^{\pm}$ (*Y09*), yielding the same modeled shoreline. Fairly wide variations in parameter values may produce similar results.

Alongshore-averaged model coefficients broadly represent site-specific free-parameter values for bulk comparison to *Y09* (Table 2.3). Alongshore averaged, C^{+} had the greatest disparity (more than double in magnitude) relative to *Y09* 5-year calibrated C^{+} at Torrey Pines. However, as noted previously, the model is not sensitive to parameter values, with C^{+} being the least sensitive parameter and can span up to a factor of four from an optimal value with no more than a 10% increase in RMSE (*Y09*). Thus, factor of two differences in C^{+} are not necessarily remarkable.

2.6.3 Alternative model formulations

Davidson et al. (2013) and Splinter et al. (2014) use an equilibrium model with forcing governed by wave power (rather than wave energy, E, in (2.2)) and the Dean parameter, which depends on grain size. The range of sand grain sizes is not taken into account here, and is relatively small (4 of the 5 beaches have D_{50} between 0.15-0.18 mm, (Table 2.1)). At Torrey Pines, *Y09* showed that replacing wave energy, E, in their shoreline model with H_s or radiation stress S_{xx} resulted in similar model skill,

because E, H_s, and S_{xx} are strongly mutually correlated. Davidson et al. (2013) and others use an equilibrium condition based on the weighted average of antecedent waves, rather than on the present beach state. However, the present beach state depends on the previous wave conditions, and for the idealized case of a step change in time to a constant wave forcing, the equilibrium conditions of Davidson et al. (2013) and *Y09* yield identical results. These different equilibrium models were also shown to yield similar results for the field observations (Castelle et al., 2014).

The basic equilibrium equation of the present model (2.2), with a linear dependence of dS/dt on the present wave energy E, and 4 free parameters, is referred to as the linear$_4$ model (the subscript specifies the number of free parameters). Additional alternative models are linear$_3$, exp$_4$, and cubic$_4$. The linear$_3$ model reduces the number of free parameters to three by replacing $C^{\pm}$ with single valued C in (2.2a) (following Yates et al., 2011). The exp$_4$ and cubic$_4$ alternative models also simplify $C^{\pm}$ with C in (2.2a), but use more complex forms of E_{eq},

$$E_{eq} = a_0 e^{a_1(S-a_2)} \quad \text{for exp}_4 \tag{2.4}$$

and

$$E_{eq} = a_0 + a_1 S + a_2 S^3 \quad \text{for cubic}_4. \tag{2.5}$$

The model parameters S_{eq} and E_{eq}, the rate of change dS/dt, and the response time τ, are similar in the range of common S and H_s, but differ at the extremes (Figure 2.10). All models use the same erosion limiter S_{bb}.

Overall (2003-2011) the alternative models perform similarly, with typically small (<15%) improvements in model error relative to the *Y09* model, which has no erosion limiter (Figure 2.9c). Model performance varied by site, but explained more

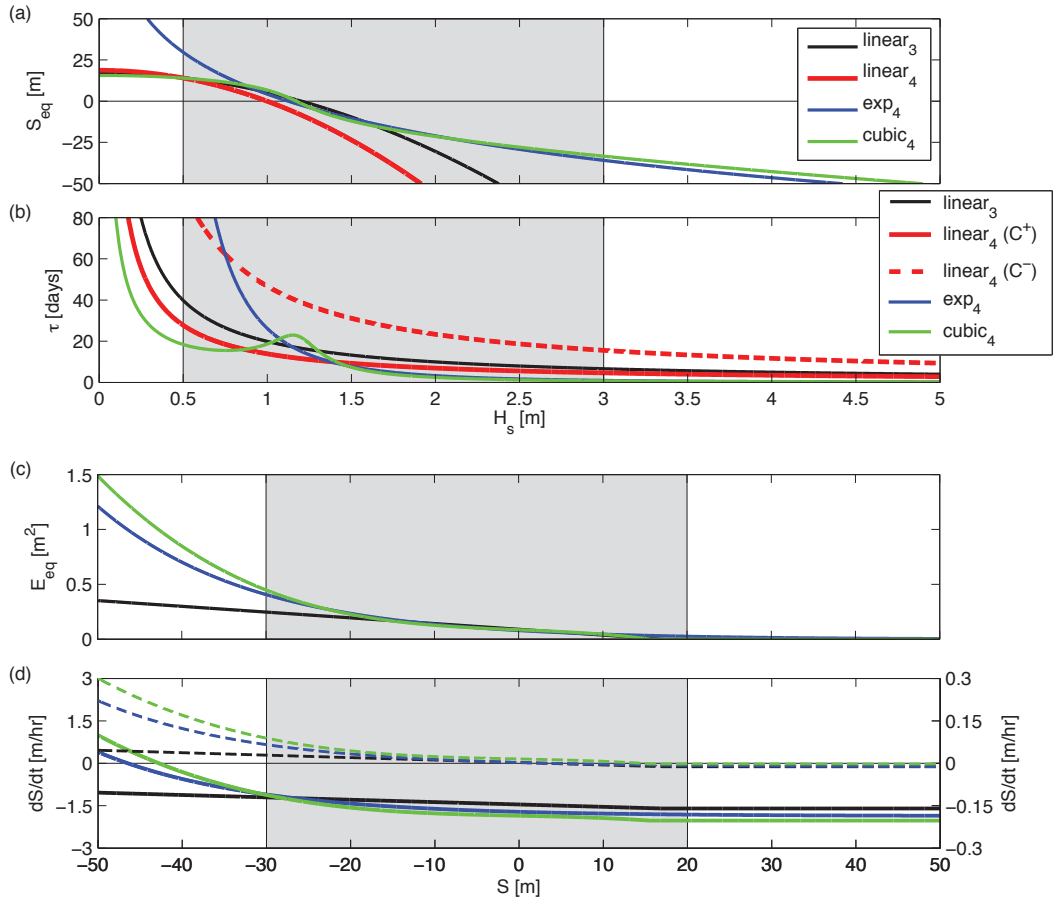

Figure 2.10: Example model results for Torrey Pines section T8 parameters: (a) equilibrium shoreline position S_{eq}, and (b) characteristic response time scale τ, both versus significant wave height H_s. See legend for model types. (c) Model E_{eq} and (d) shoreline change rate dS/dt, both versus shoreline position S. An accreted beach has $S > 0$ and an accreting beach has $dS/dt > 0$. In (d), results are shown for high ($H_s = 4$ m; solid curves; left vertical axis) and low (H_s = 0.4 m; dashed curves; right vertical axis) energy waves. Shading indicates the range of commonly occurring H_s and S.

than 50% of the variance over 16 years at most of the sandy beaches, similar to *Y09* five-year hindcasts. The models differ from the *Y09* model most significantly for extreme conditions only briefly encountered. While the *Y09* model correctly identifies the 1997-98 waves as more erosive than 2009-10, it overestimates shoreline erosion during both El Niño events.

The cubic_4 model provided the greatest improvements in model skill (relative to *Y09*), with improved predictions for El Niño 2009-10 at beaches both where the erosion limiter was and was not reached (Solana Beach and Torrey Pines, respectively, Figure 2.9a,b). The over-prediction of the winter 2009-10 shoreline erosion (Δ_{W10}, Figure 2.9d) was reduced using the cubic_4 model at all sites except Camp Pendleton, where over-prediction persisted. Model-data comparison at Camp Pendleton was generally poor irrespective of which model was used, perhaps owing to the close proximity of a river mouth. Typical Δ_{W10} reductions are about 5 m (up to 18 m peak reduction) relative to *Y09*. With large waves (H_s = 4 m) and a heavily eroded shoreline (solid curves, S = -40 m, Figure 2.10d), dS/dt for $\exp_4$ and cubic_4 are much smaller in magnitude than for linear_3 (a simplified version of the *Y09* model). Physical processes that reduced beach face mobility include the exposure of resistant strata and/or the reduction of wave energy reaching the beach face by breaking on well-developed offshore sandbars.

Using the χ^2 based goodness-of-fit metric, Q (Press et al., 2007), as a model performance measure, with degrees of freedom based on the decorrelation scale (Davis, 1976), the improvement in overall fit provided by the added cubic term in the

cubic$_4$ model was commonly more statistically significant than the linear$_3$ model. Q values for these models, which ranged from 0.35 to 0.99, were all above the goodness-of-fit threshold suggested by Press et al. (2007) (e.g. $Q > 0.1$). Most notably, the goal of reducing erosion over-prediction during rare energetic events, by inclusion of a cubic term, is achieved (Figure 2.9d; green markers).

2.7 Conclusion

Sixteen years of shoreline and wave observations, including two El Niños 1997-98 and 2009-10, illustrate seasonal and long-term fluctuations in wave climate and shoreline sand levels at five southern California beaches. An existing, empirical shoreline model driven with hourly wave conditions simulates well the seasonal changes in subaerial beach width (e.g. the cross-shore location of the MSL contour) during non-El Niño years, similar to previous results (*YO9*). During El Niño winters the *Y09* model over-prediction of shoreline erosion is reduced by including the location of erosion resistant boundaries (identified with aerial images), and using alternative, nonlinear forms of E_{eq} (e.g. cubic$_4$) that gradually decrease the mobility of highly eroded shorelines (simulating cobbles, kelp wrack, enhanced offshore sand bars, and other stabilizing effects).

The shoreline location depends on complex processes occurring over the cross-shore beach profile, and in some cases on adjacent profiles. Even significantly different equilibrium shoreline models often have similar skill (Castelle et al., 2014), which is also true for existing, more computationally demanding, physical process models for shoreline change. Application of any model to extreme conditions on sand-

limited beaches with unknown substrates will requires site and condition specific calibration. Once trained, the present model provides a computationally simple (e.g. nonlinear first order differential equation) representation of the observed relationship between incident waves and shoreline change, including the effect of erosion resistant substrates.

Acknowledgements

This research was supported by the United States Army Corps of Engineers and the California Department of Parks and Recreation Division of Boating and Waterways (program manager Reinhard Flick). The paper was substantially improved by reviewer and editor comments. André Doria was supported by Fellowships from the University of California Regents, NDSEG, and the National Science Foundation (GRFP). SANDAG, Coastal Frontiers Corporation, and Fugro are thanked for their assistance in using their datasets. This publication was prepared by André Doria under NOAA Grant #NA10OAR4170060. California Sea Grant Project R/RCC-01, through NOAA's National Sea Grant College Program and the U.S. Dept. of Commerce. The statements, findings, conclusions and recommendations are those of the author(s) and do not necessarily reflect the views of the aforementioned organizations.

The text of Chapter 2, in full, is a reprint with minor modifications of the paper "Observations and modeling of San Diego beaches during El Niño," *Continental Shelf Research*, 124, 153-164, http://dx.doi.org/10.1016/j.csr.2016.05.008 (Copyright of Elsevier Ltd. 2016). The dissertation author was the primary researcher and first author with guidance provided by R.T. Guza, William C. O'Reilly, and M. L. Yates.

3

Regional variability and modeling of Southern California beach sand levels

3.1 Abstract

Subaerial beach sand levels were observed along 195 km of southern California coast with twenty airborne lidar surveys between 1998 and 2010. Shoreline change was largest during the 1997-98 and 2009-10 El Niños. In the southern half, as observed previously, the many reaches of uninterrupted shorelines erode in winter, when wave energy is highest. Further north, geological features and jetties on the crenulated shoreline often control beach response. The winter shoreline can accrete near jetties and headlands, from mechanical berm building, and when the shoreline in pocket beaches rotates in response to seasonal changes in wave direction. Additional biannual in situ surveys (1997-2012) distributed over the southern 90 km were joined with the lidar surveys to calibrate an existing, simple equilibrium shoreline change

model. The model performance varied alongshore, but explained more than half the variance at 2/3 of the 21 test sections, with all locations being significant at the 95% level. A single set of shoreline change model free parameters performed almost as well as parameters tuned locally to each individual beach section, and provide a simple, generic shoreline change model for sandy reaches within this 90 km span.

3.2 Introduction

Sand level changes at beaches throughout the Pacific Rim have been linked to decadal scale variations in ENSO climate indices (Barnard et al., 2015). During strong El Niños, unusually large erosion is observed at many Pacific Rim beaches, with significant socio-economic and ecological impacts (Zhang et al., 2004; Nicholls et al., 2007; Revell et al., 2011). Erosion on the US West Coast is increased by ENSO-related elevated water levels and changes in storm frequency, intensity, and track (Allan and Komar, 2006; Ruggiero et al., 2010a). Independent of long-term (centuries) sea level rise, more intense and/or frequent El Niños could increase near-term (decadal) coastal erosion at many locations on the US West coast (Cai et al., 2014, 2105; Barnard et al. 2015).

Airborne light detecting and ranging (lidar) can measure the subaerial (above the waterline) sand elevation over hundreds of kilometers in a single day, with point density and accuracy that resolves significant changes (Brock et al., 2002; Stockdon et al., 2002; Sallenger et al., 2003; Reineman et al., 2009). Airborne lidars have been used to monitor beach nourishments (Gares et al., 2006), flood control berms (Gallien et al., 2015), hurricane inundation vulnerability (Stockdon et al., 2009), coastal dune

and cliff changes (Sallenger et al., 2004; Young et al., 2006), and beach change (Krabill et al., 2000; Sallenger et al., 2003, Doria et al., 2016).

On the U.S. West Coast, lidar surveys have been used to examine erosion during the 1997-98 El Niño (e.g. Revell et al., 2002, 2011). At a few west coast beaches, in situ and lidar surveys have been combined, and erosion estimated during the 1997-98 and/or 2009-10 El Niños (Barnard et al. 2011; Revell et al., 2011; Doria et al., 2016). The alongshore span of the southern California beaches in each of these studies was small, totaling less than 20 km, and were concentrated in the southern half of the present study region. One study site, Torrey Pines Beach, is described extensively in the historical literature, using a few cross-shore transects (Nordstrom and Inman, 1975; Winant et al., 1975; Aubrey, 1979; Aubrey et al, 1980). At these selected sites, erosion and wave energy are maximum in winter, and shoreline erosion is strongest during El Niño winters. Here, we examine the alongshore variation of shoreline response in El Niño and non El Niño years over 195 km of southern California coast, from the U.S.-Mexico border to Los Angeles, using twenty airborne lidar surveys collected between 1998-2010.

Wave and sand level observations are described in Section 3.3. Alongshore variations in sand levels over the 195 km are discussed in Section 3.4. In Section 3.5, supplemental shoreline data collected on transects spanning the southernmost 90 km (San Diego County) are combined with the lidar observations to test an existing wave-driven equilibrium shoreline model. In Section 3.6, the similar response of the southern beaches is shown to support use of a single set of beach response model

parameters. Section 3.7 is a summary.

3.3 Observations

3.3.1 Waves

A network of directional wave buoys (http://cdip.ucsd.edu) was used to estimate surface waves. Open-ocean swell wave buoys (0.04-0.1 Hz; triangles in Figures 1b and 2b) and offshore sea wave buoys (0.08-0.5 Hz; squares) initialized a spectral refraction wave model (O'Reilly et al, 2016) that provided hourly near-shore (~10 m depth) wave estimates every 100 m over the 195 km study region. The wave model has been validated with shallow (~25 m depth) near-shore buoy deployments at several locations within the study site (Young et al., 2012; O'Reilly et al., 2016). Wave estimates near atypical, complex local bathymetry or structures (e.g. harbor entrances and interiors, prominent jetties and breakwaters) were discarded.

In southern California winter, energetic waves come from northwest Pacific storms. Summer is often dominated by lower energy long swell from the south Pacific. Wave conditions vary alongshore owing to changing coastline orientation and shadowing from the offshore Channel Islands. The annual average shallow-water (~10 m depth) H_s generally decreases northward as the coastline orientation turns from west facing to south facing (Pawka, 1983).

At the Oceanside buoy, broadly representative of the southern half of the study region, the El Niño winters of 1997-98 and 2009-10 are most prominent for the relative frequency of significant wave heights H_s, greater than 2 m ($H_{s,>2}$) (Figure 3.3a). The directional-frequency wave energy distributions for waves with $H_{s>2}$ were

summed for each winter (defined as November through March) and then normalized by the 2010 El Niño maximum value. Compared with average (Figure 3.3b) and moderate (Figure 3.3d) winters, El Niño winters (Figure 3.3c,e) have more energetic seas (0.15-0.25 Hz) from a range of directions, and higher swell (0.07-0.15 Hz) from the westerly direction that, at Oceanside, is unobstructed by offshore islands.

3.3.2 Sand Levels

195 km. Subaerial beach sand levels were observed with twenty airborne lidar surveys from the US-Mexico border to Long Beach, a distance of approximately 195 km (Figures 1, 2). The first lidar survey (April 1998) measured erosion from the 1997-98 El Niño. From May 2002 through October 2010, biannual lidar surveys generally occurred in October and March. Lidar returns landward of the back beach (e.g. cliff base, coastal revetments) and seaward of the waterline were eliminated (Yates et al., 2008). The remaining subaerial beach data were gridded onto a 4 m^2 cell grid retaining the cell median elevation value to remove sporadic outliers (e.g. birds, beachgoers, and erroneous returns). Survey cell grids with less than 3 data points were excluded, except for the low density 1998 lidar survey; ~0.57 points m^{-2} compared with the post-2002 surveys (~2 points m^{-2}). Elevations were extracted on 5 m widths about cross-shore beach transects spaced 100m alongshore and co-located with the near-shore wave estimates.

Note that changes in beach bathymetry, not captured by the subaerial lidar surveys, may be important in assessing seasonal sand level changes. In fact, subaerial beach face changes account for as little as 10-20% of the total beach face eroded

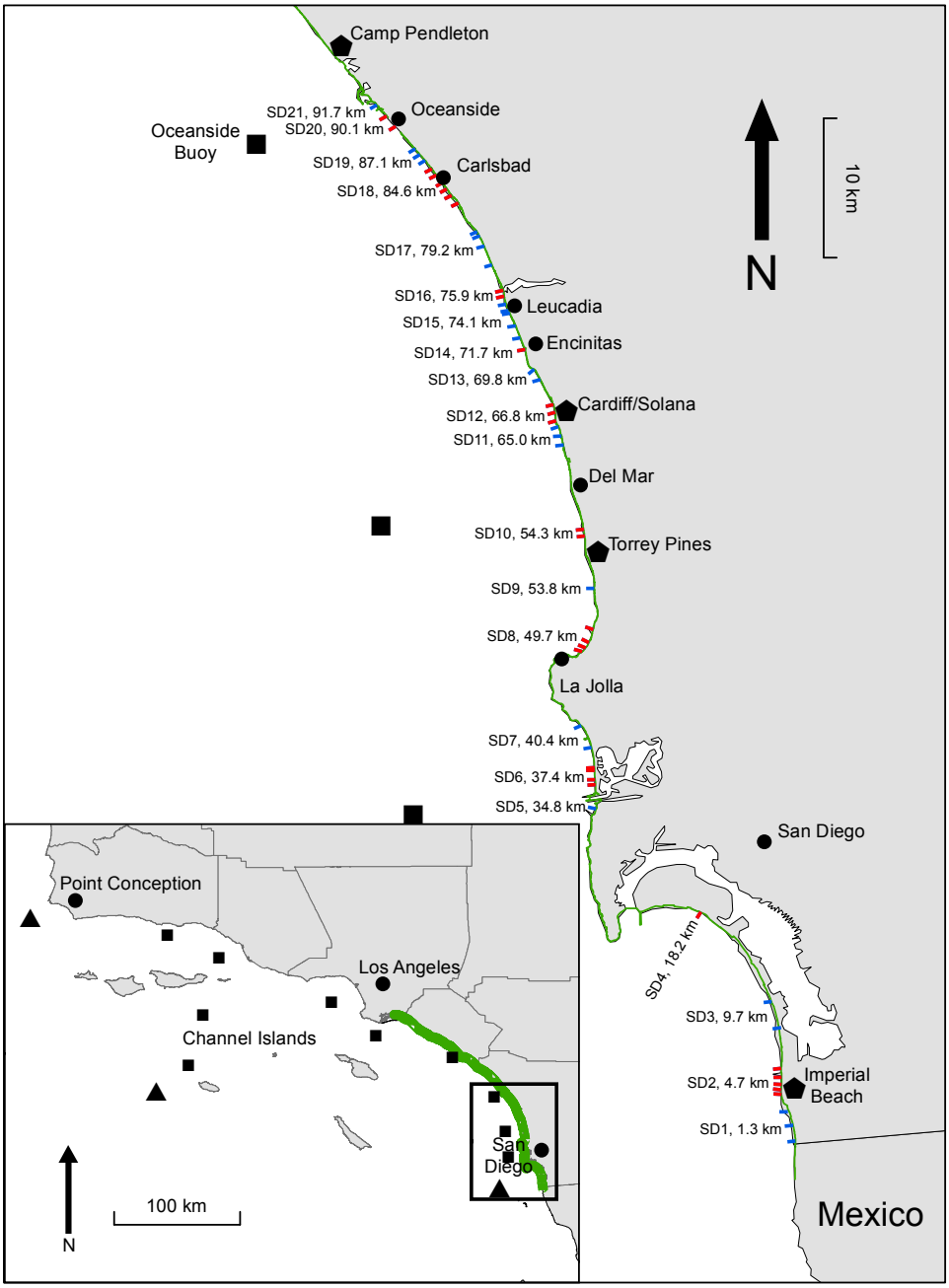

Figure 3.1: Maps of southern California with subaerial lidar coverage indicated with green curves. The region within the bold black frame in the inset (b) is expanded in (a). Cross-shore transects were surveyed on 57 lines (blue and red lines) spread over the region in (a). Focus sites used in Doria et al. (2016) are indicated (pentagons). San Diego county model section numbers (SD) and alongshore distance (km) from the Mexico-U.S. border are indicated. Offshore regional swell (black triangles) and sea (black squares) wave buoys are shown. Nearshore (~10 m depth) 100 m alongshore-spaced hourly wave estimates span the entire lidar coverage region.

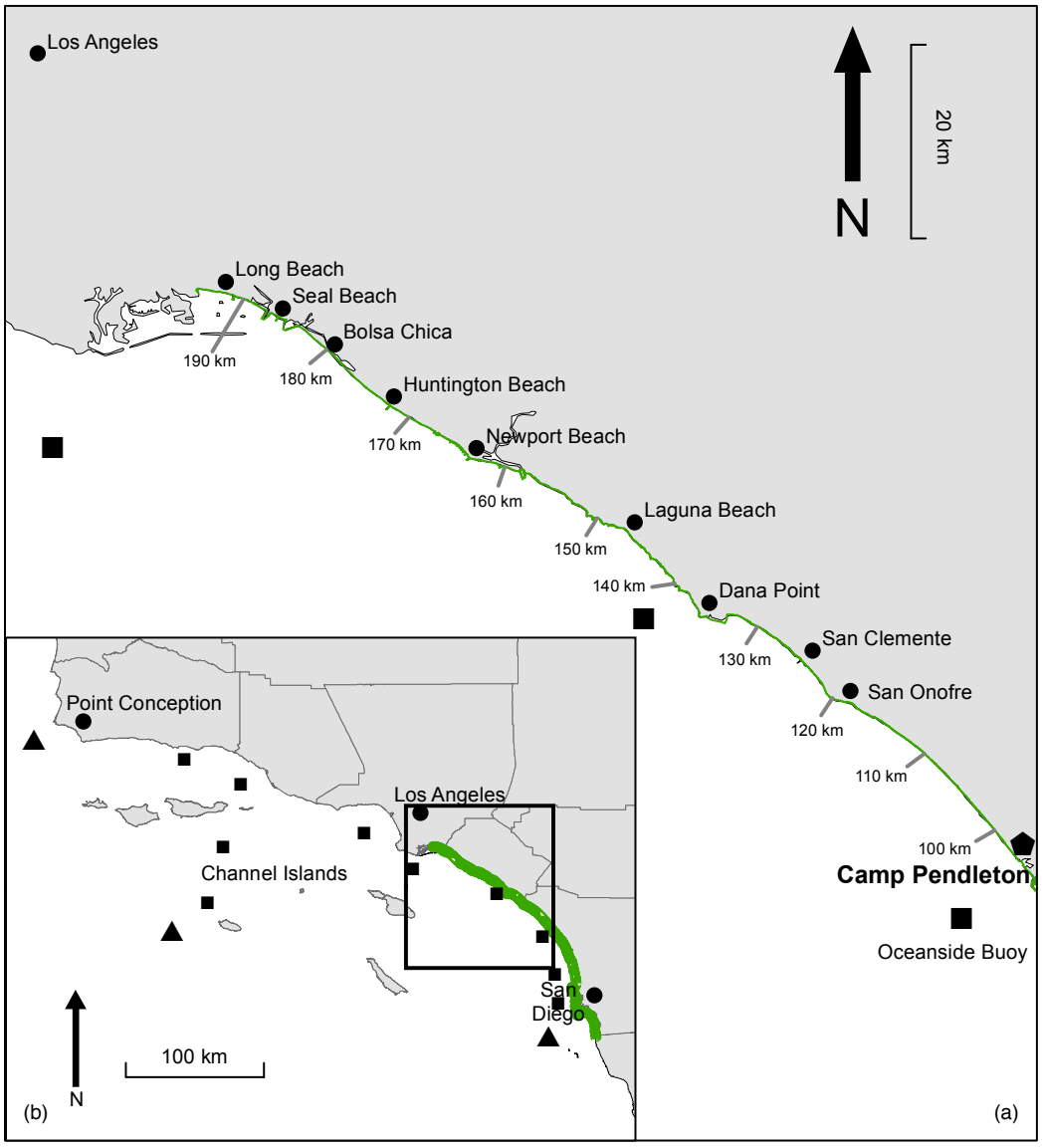

Figure 3.2: Maps of southern California with subaerial lidar coverage indicated with green curves (same format as Figure 3.1). The region within the bold black frame in the inset (b) is expanded in (a).

volume (e.g. subaerial and bathymetric profile changes) during energetic winters (Doria et al., 2013).

South 90 km. The San Diego Association of Governments (SANDAG) sponsored biannual beach sand levels surveys, using traditional survey methods, on 57 cross-shore transects distributed over the southern 90 km (Figure 3.1) from 1997 until 2012 (Coastal Frontiers Corporation, 2016). Subaerial lidar data was extracted on these same cross-shore transects, forming an overlapping and continuous 15 year time series (Figure 3.8, discussed below). Specifically, the 1999-2002 gap in lidar is filled with the SANDAG in situ observations.

3.4 Results

3.4.1 Sand Level Changes over 195 km

The time-averaged average seasonal beach widths, the cross-shore span from the back beach to the time-averaged shoreline (MSL) location, vary significantly alongshore. The widest beaches are located at Coronado and Camp Pendleton in the south (Figure 3.4a; 12-21 km and 92-96 km, respectively), and in the north (Figure 3.4d) from Newport Beach to Huntington Beach (160-174 km), and Seal Beach to Long Beach (183-195 km). Beach widths varied seasonally with root-mean-square (RMS) fluctuations of 5-15 m (Figure 3.4a,d; gray curve). Narrow beaches, between 5-20 m wide, were often rocky, wave-cut platforms, with armored steep cliffs. Reflecting their durable composition and limited sand, these beaches had low seasonal RMS shoreline fluctuations (~2-3 m, Figure 3.4a; 24-34 km and 42-45 km).

Beach slopes, estimated at MSL, also varied seasonally with steepened winter

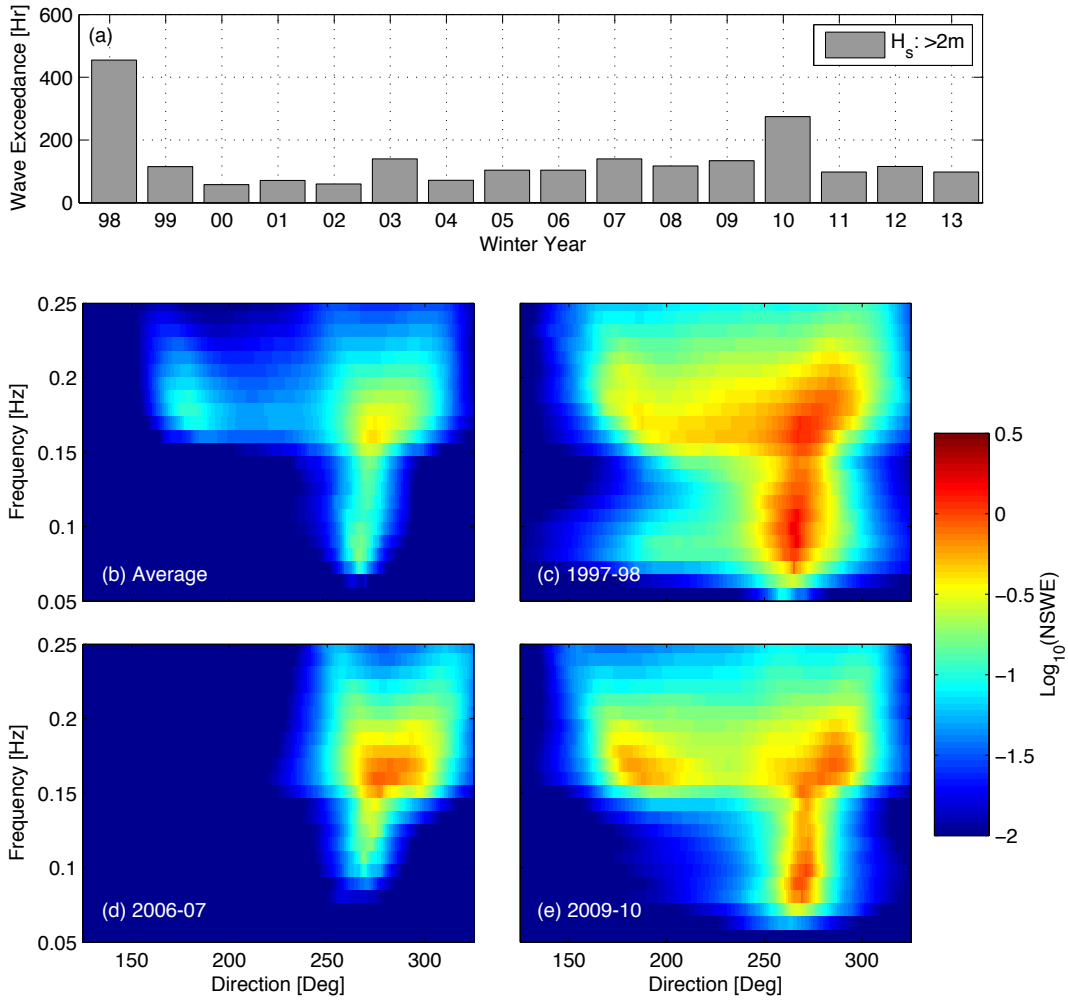

Figure 3.3: (a) Hours of observed H_s greater than 2 m versus winter year (November-March) from November 1997 through March 2013 at Oceanside Buoy. Normalized summed hourly winter (November through March) wave energy (NSWE) frequency-direction spectra at the Oceanside Buoy (Figure 3.1a) for $H_s > 2$ m (b) average of winters (1997-98 through 2012-13), (c) 1997-98 El Niño winter, (d) 2006-07 winter, and (e) 2009-10 El Niño winter. Spectra are normalized by the summed hourly El Niño 2010 winter wave energy maximum, 0.16 m^2 $Hz^{-1}Deg^{-1}$.

foreshores (Figure 3.4b,e). Sandy beach slopes are usually < 0.05, with a general trend of northward increasing beach slope (compare Figure 3.4b with 3.4e; note vertical axis differ). Mean sediment size also increases northward (0.15-0.40 mm) (Yates et al.,

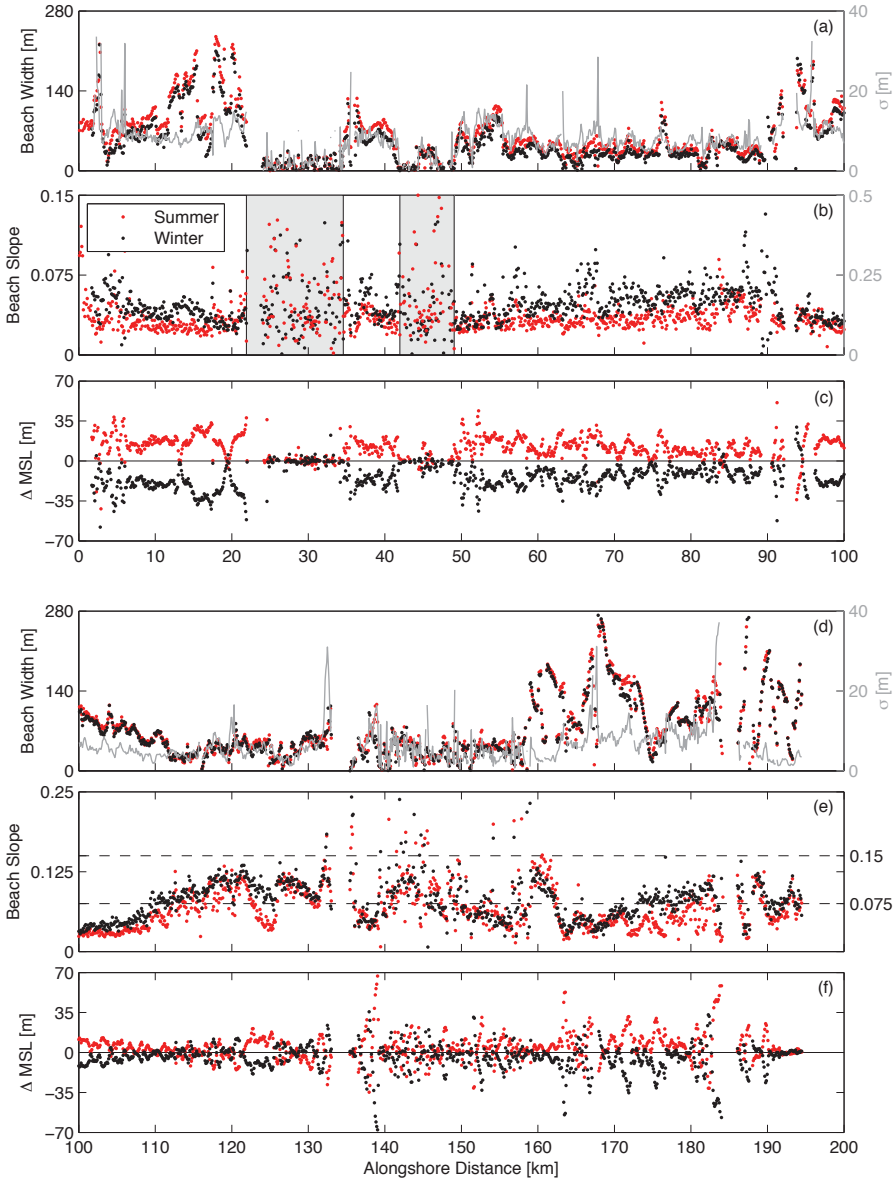

Figure 3.4: 1998-2010 average summer and winter (a) cross-shore beach width (black and red markers; left axis) and seasonal cross-shore beach width standard deviation (gray curve; right axis), (b) beach slope, (c) cross-shore MSL change versus alongshore distance (0-100 km). Summer (winter) values are indicated by red (black) markers. Shaded alongshore regions in (b) are exceptionally steep regions and correspond to the right vertical axis. (d)-(f) as above, but for alongshore distance 100-200 km. Black horizontal dashed lines in (d) indicate mid and max vertical axis values in (b). Alongshore distance increases northward. Beach width is the cross-shore distance from the back beach to the average summer (winter) MSL contour location.

2009b). Rocky beach faces and high relief bluffs had widely variable slopes (Figure 3.4b; shaded regions), including slopes higher than 0.25.

Time-averaged (1998-2010) seasonal shoreline excursions, ΔMSL , (e.g. summer to winter retreat and vice-versa) vary alongshore, and approximately balance at each location (Figure 3.4d,f). In the southern 90 km (e.g. San Diego County), several long uninterrupted sandy beaches generally behave qualitatively similarly, with the strongest shoreline erosion coinciding with winter, especially El Niño winters (e.g. Barnard et al. 2011; Doria et al., 2013; Doria et al., 2016). In the south, seasonal changes have the same sign at most alongshore locations, and the alongshore-averaged (averaged within four 50 km alongshore sections noted in Figure 3.5) cross-shore location of the shoreline (MSL position) equals the alongshore average of the absolute value of the shoreline fluctuations (MSL magnitude) (compare circles and triangles in Figure 3.5). Further north, where shoreline change has not been well documented, the average winter shoreline accretes in many locations. The two change metrics (e.g. MSL position & MSL magnitude) are notably unequal in 100-150km (Figure 3.5c), and differ somewhat in 150-195 km (Figure 3.5d). MSL magnitude extremes for winter occurred during the 1997-98 and 2009-10 El Niños (dashed vertical grey lines, black circles) in all 4 sections. Note, because accretion and erosion were effectively equal, the average change in 100-150 km was near zero.

The northern shoreline is crenulated with pocket beaches, submarine canyons (e.g. Everts and Eldon, 2005), and many shoreline engineering structures associated with coastal development (Griggs et al, 2005, Patsch and Griggs, 2006). Winter

accretion occasionally occurs near structures and headlands, from mechanical berm building, and when the shoreline in pocket beaches rotates in response to seasonal or episodic changes in wave direction, as observed elsewhere (Komar and Inman, 1970; Inman and Brush, 1973; Thomas et al., 2011).

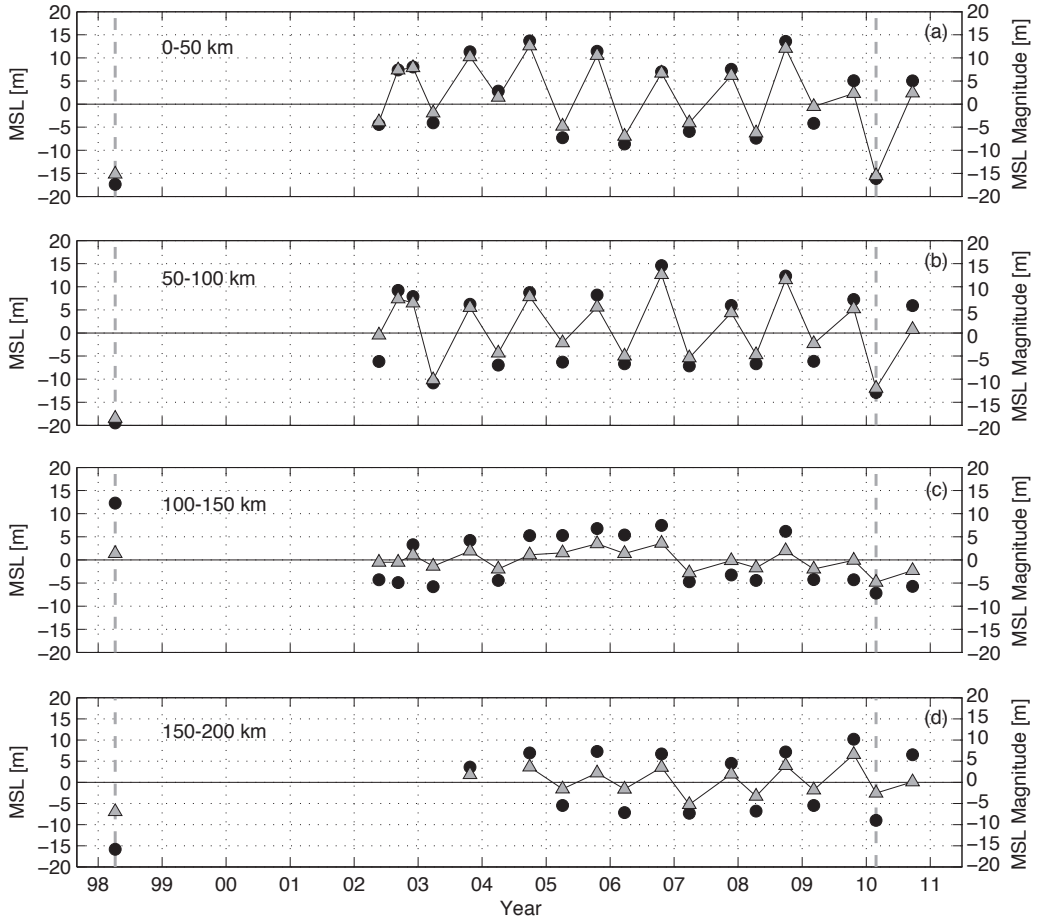

Figure 3.5: Demeaned and alongshore averaged MSL cross-shore position (left axis; triangles) versus time (ticks are 1 January). Positive values correspond to a relatively wide subaerial beach. MSL magnitude (right axis; black circles) is the corresponding MSL position from alongshore averaging the absolute values of MSL. MSL magnitude is multiplied by the sign of the average MSL position value to improve visual comparison. Values averaged over alongshore distances (a) 0-50 km (b) 50-100 km (c) 100-150 km, and (d) 150-200 km. Alongshore distance increases northward (Figures 3.1 and 3.2). MSL magnitude extremes occurred during the 1997-98 and 2009-10 El Niños (dashed vertical grey lines, black circles).

The overall patterns of spatial variability in time-averaged results (Figure 3.4) also occurred during the El Niño 2009-10 winter. North of 130 km, 25% of the shoreline accreted, in several locations more than 25 m horizontally and 2 m vertically (Figure 3.6d,e). At Newport Beach (161-163km), groins and jetties interrupt the longshore transport, causing accretion on the updrift side (Figure 3.7a, Storlazzi and Field, 2000).

Many pocket beaches (e.g. headland confined shores of short alongshore span) pepper the coast from Dana Point northward (135-158 km), including Laguna Beach (Figure 3.7b). These natural coastline features reduced alongshore transport and the interaction between adjacent beaches, resulting in alongshore alternating oscillating sand levels. Note also that during 1997-2013, the average winter H_s usually was larger than the average summer H_s in the southern ~85 km. However, seasonal differences narrow further north, and summer waves were actually larger than in winter along a 19 km stretch (153-172 km).

Sunset Beach (177-184 km), a reach lacking visible cross-shore structures, exhibited sand level elevation oscillations exceeding ±3 m over relatively short (O(0.3-1 km)) alongshore spans (Figure 3.7c). This unusual behavior was found in all survey years with the polarity of the changes alternating seasonally, coherent with seasonal changes in wave climate. The alongshore-oscillating pattern in sand level change may be partially associated with a winter berm (1 km long, ~1-2 m tall, ~6 m^3/m) constructed annually to protect beachfront property, and regraded in spring (Gallien et al., 2015). Detailed time series of beach sand levels, and of berm building

and beach scraping, would be needed to explain the unique sand level changes at Sunset Beach.

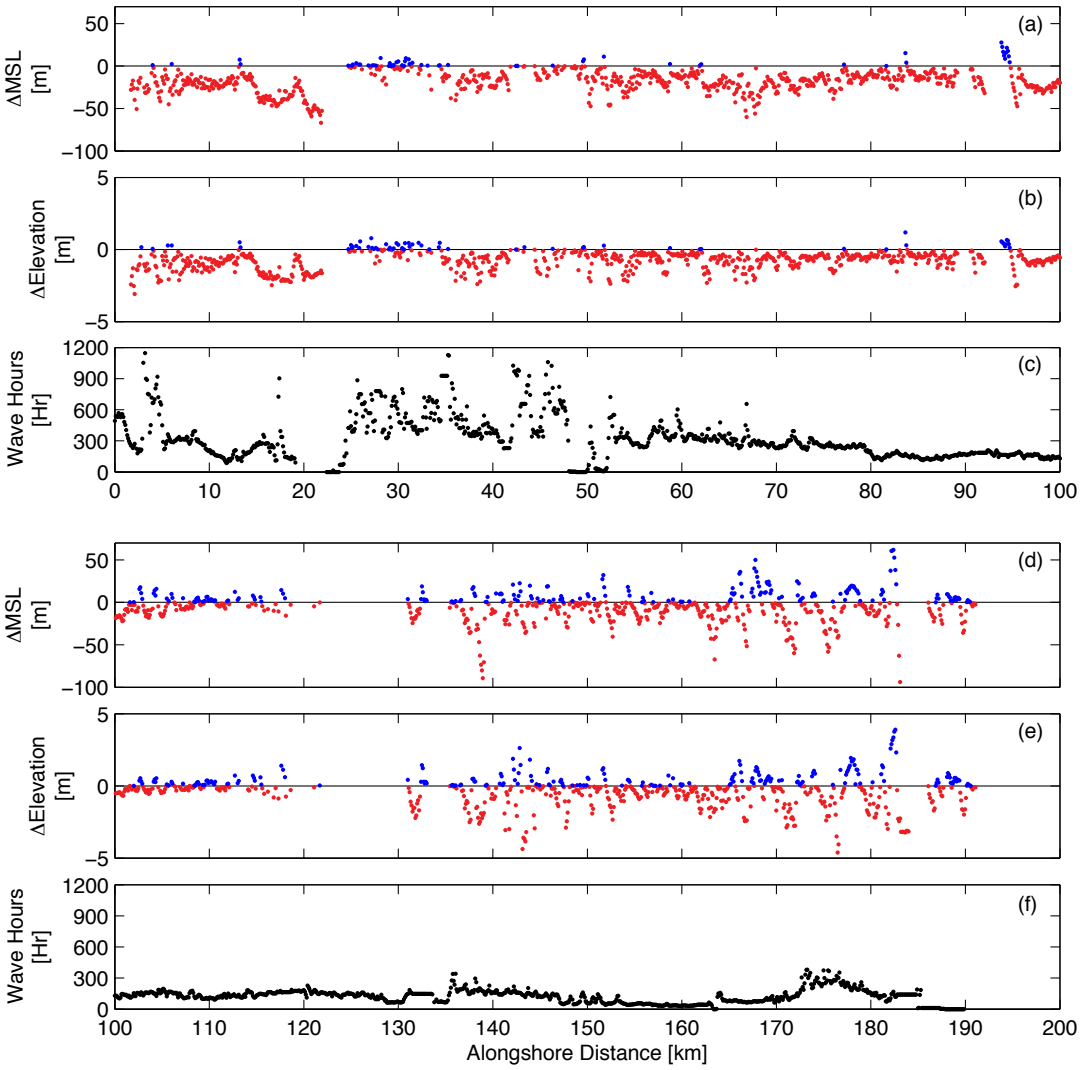

Figure 3.6: Fall 2009 to El Niño 2010 winter (a),(d) cross-shore MSL change and (b),(e) elevation change at the most retreated MSL cross-shore location, (c),(f) hours (November 2009 through March 2010) of $H_s > 2$ m versus alongshore distance. Negative (erosive) beach changes are red, and positive (accretion) changes are blue.

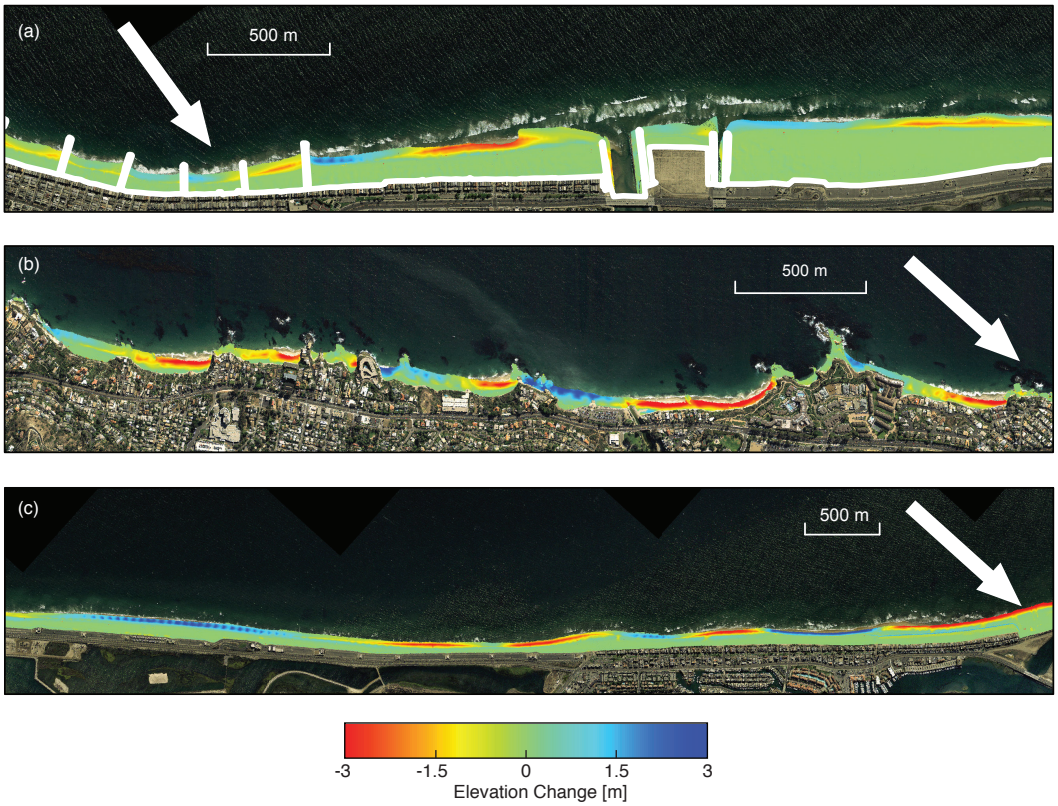

Figure 3.7: Plan view of elevation change near (a) groins and jetties, Newport Beach (164.7-169.0 km), (b) pocket beaches, Laguna Beach (144.6-146.6 km), (c) actively managed Sunset Beach (177.0-183.9 km). North arrows are shown.

3.5 Regional shoreline modeling

Observed shorelines were hindcast for 15 years at 21 locations spanning the San Diego coastline using an existing equilibrium shoreline model (Doria et al., 2016). Equilibrium shoreline models hypothesize that the cross-shore shoreline rate of change, dS/dt, is related to the incident wave forcing and the present beach state (Wright et al., 1985). Several stretches (O(1-7 km)) of southern California beach show

equilibrium behavior of the shoreline (Yates et al., 2009a) and beach profile (Ludka et al., 2015).

Doria et al. (2016) extended Yates et al. (2009a) to account for non-erodible back beach substrates and boundaries. With the shoreline position S defined as the cross-shore location of MSL, dS/dt is proportional to the significant wave height $\left(H_s \propto E^{1/2}\right)$ and the wave energy disequilibrium ΔE,

$$\frac{dS}{dt} = \begin{cases} CE^{1/2}\Delta E(S) & \text{for } S > S_{bb} \\ 0 & \text{for } S \le S_{bb} \end{cases}, \tag{3.1a}$$

where C is the empirically determined change rate coefficient, S_{bb} is the cross-shore location of the non-erodible back beach (e.g. cliff, rock outcropping) and the wave energy disequilibrium is

$$\Delta E(S) = E - E_{eq}(S). \tag{3.1b}$$

E_{eq}, the equilibrium wave energy, is the incident wave energy for a given S that yields no shoreline change. Yates et al. (2009a) used an E_{eq} linearly related to the shoreline position S that sufficed for typical winter wave climates encountered in their ~5-year hindcast. As demonstrated by Doria et al., (2016), overprediction of erosion in extreme events (El Niño) in a 16-year data set is amelorated using

$$E_{eq}(S) = a_0 + a_1 S + a_2 S^3 \tag{3.2}$$

where a_0, a_1, and a_2 are empirically determined coefficients. The cubic form of E_{eq} coarsely accounts for reduced erodibility when resistant layers (cobbles, shell hash, peat) are exposed. While different dimensional and non-dimensional forcing

parameters have been used to drive empirical equilibrium shoreline models (3.1a), wave energy, E, typically performs well (Davidson et al., 2010, 2013; Castelle et al., 2014; Splinter et al., 2014).

The SANDAG cross-shore transects were modeled by subdividing the 57 transects into 21 alongshore-averaged sections (Figure 3.1a) based on geographic proximity and local environmental factors (e.g. headlands, artificial and geological barriers, fluvial features). Excluding four sections based on a single transect, modeled sections spanned 0.4-2.9 km alongshore with an average inter-section transect spacing of 420 m. Note there are significant spatial coverage gaps througout the San Diego coastline in the SANDAG transect locations (Figure 3.1a). The combined SANDAG and lidar shoreline observations (extracted along the SANDAG transects and temporally demeaned) and the back beach limit S_{bb} locations were alongshore averaged within each section. Hourly wave estimates located in each section, within 250 m alongshore of each transect, were also alongshore averaged. Using these averaged intermittent shoreline observations and hourly wave estimates, surrogate management framework optimization (Booker et al., 1999; Marsden et al., 2004), a derivative-free method that can negotiate local minima, determined the four model free-parameters $\left(C, a_0, a_1, a_2\right)$ at each alongshore section by minimizing the model-data root-mean-square error (RMSE). The model calibration period was summer 2003 to fall 2011 (Doria et al., 2016).

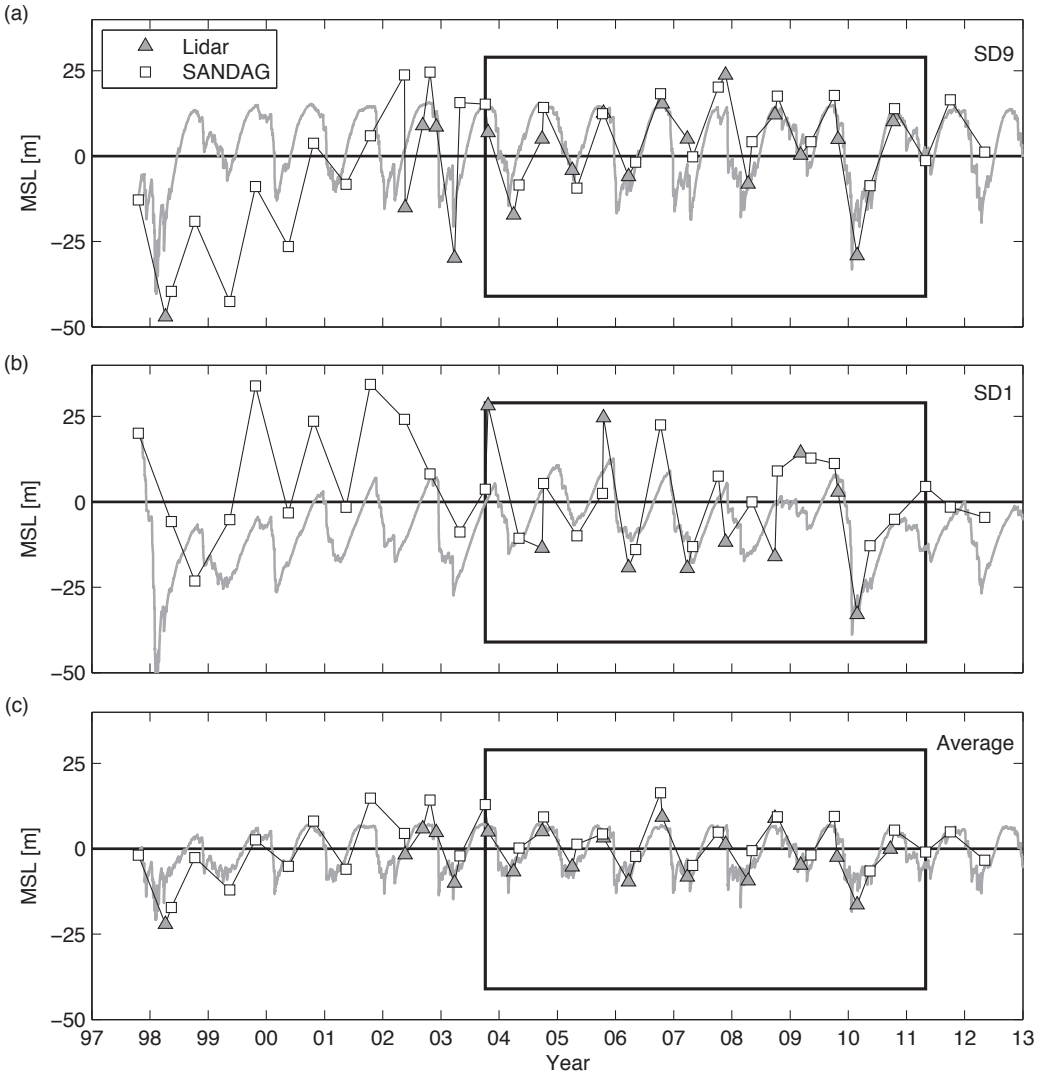

Figure 3.8: Modeled and observed MSL position versus time (ticks are 1 January) for representative modeled sections (a) SD9 (Torrey Pines), (b) SD1 (Tijuana River mouth), and (c) average San Diego. Shoreline observations (squares and triangles; data source indicated in legend), model prediction (gray curve), and model calibration period (black rectangle) are shown. Model root-mean-square errors (R^2) are (a) 13.2 m (0.46), (b) 17.3 m (0.26), and (c) 4.7 m (0.69).

Shoreline hindcasts were initialized with the SANDAG October 1997 observations. Model skill (R^2), defined as $\left(\frac{\langle xy \rangle}{\sigma_x \sigma_y}\right)^2$, ranged from 0.14 to 0.77 across

sites with an average of 0.52; however, the majority of the sites had skill greater than 0.56 (Figure 3.9a). Model RMSE for the entire observation period was generally between 5.3-11.7 m (Figure 3.9a), only marginally higher error (by ~1 m) than similar long-term shoreline modeling at select focus beaches in San Diego calibrated primarily with monthly observations (Doria et al., 2016). Locations with relatively low skill (and large RMSE) were often adjacent to lagoon or river mouths, and received fluvial sediment or opportunistic nourishments not included in the model.

The observed October 1997 beach widths, used to initialize the model, were markedly retreated compared to typical pre-winter shorelines (Figure 3.8a,c). Accordingly, the 1997-98 El Niño winter had the most significant modeled erosion. Following the 1997-98 winter, modeled shorelines recovered by the proceeding summer, more rapidly than the observed 3 years. After this multi-year recovery period, model-data agreement improved (Figure 3.8a).

3.6 Average shoreline model

Shoreline observations on all SANDAG transects were alongshore averaged together producing a single shoreline time series broadly representative of the San Diego region. A single set of shoreline model free parameters was generated by calibrating the countywide alongshore-averaged shoreline observations with the alongshore-averaged wave properties (Figure 3.8c). The model reproduced the averaged observations with RMSE (4.7 m) below the lowest RMSE of the 21 individually modeled sections (5.0 m).

The average model coefficients were applied to the 21-modeled sections to explore the regional sensitivity to using a single set of coefficients. Results varied alongshore, but on average RMSE increased 15% and R^2 decreased 13% when replacing the site-specific coefficients with the average model coefficients. The responses of the southern sites are similar enough to allow use of a single set of response parameters with the local waves. Other studies at focused beach sites using a similar model have shown replacement of site-specific coefficients with a single set of parameters or even notable variations in parameter values resulted in less than a 10% increase in RMSE (Yates et al., 2009a). Thus, model RMSE has a broad flat minimum in free parameter space.

The model RMSE was not sensitive to excluding the SANDAG surveys from the calibration, and vice-versa, largely due to effectively redundant model training information owing to the commonly occurring relatively small temporal separation (O(2-6 weeks)) between the SANDAG and lidar surveys (Figure 3.8).

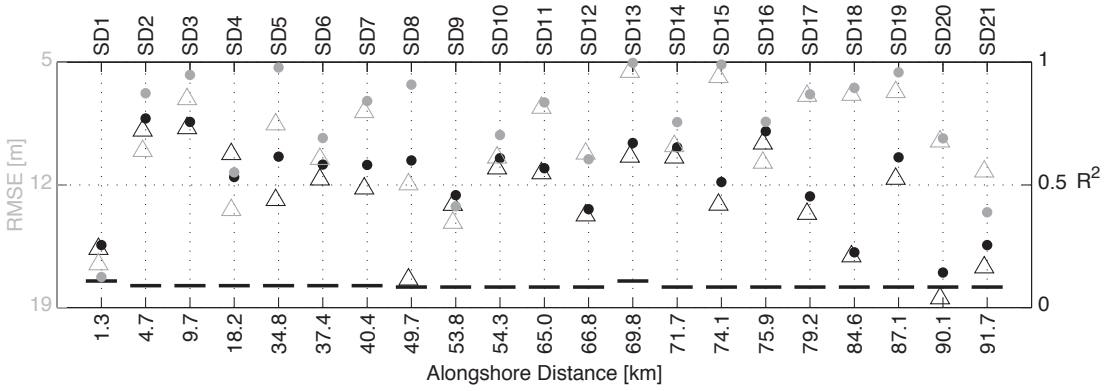

Figure 3.9: Shoreline model error RMSE (left axis; grey markers) and R^2 (right axis; black markers) for each modeled SD section (Figure 3.1a). Model performance is only slightly degraded using the average San Diego model coefficients (triangles) in place of site-specific coefficients (circles). Horizontal black bars are R^2 confidence thresholds at 95% significance.

3.7 Summary

Subaerial beach sand levels were observed along 195 km of southern California coast with twenty airborne lidar surveys between 1998 and 2010. Shoreline change was largest during the 1997-98 and 2009-10 El Niños. Alongshore variations in waves were many, but regional-scale northward decreases in H_s coincided with increased southwesterly coastline orientation and decreased magnitude of seasonal shoreline fluctuations. In the southern half, as observed previously, the many reaches of uninterrupted sandy shorelines erode in winter, when wave energy is highest, and accrete during summer lulls. Further north, the winter shoreline can accrete near jetties and headlands, from mechanical berm building, and when pocket beaches rotate in response to seasonal changes in wave direction. Additional biannual in situ surveys (1997-2012) distributed over the southern 90 km were joined with the lidar surveys to calibrate an existing, simple equilibrium model for shoreline change. The regional shoreline model successfully explained more than half the variance at a majority of the sites with 8 m average RMSE. The model failed to adequately reproduce incremental regional recovery observed after severe erosion events (e.g. 1997-98 El Niño) that resulted in multi-year sand limited conditions.

Changes in beach bathymetry, which are not captured by the subaerial shoreline surveys, may be as important as the subaerial beach for comprehensively assessing seasonal sand level changes. In fact, subaerial beach face changes have been shown to account for as little as 10-20% of the full beach profile eroded volume (e.g.

subaerial and bathymetric profile changes), especially during energetic winters (Doria et al., 2013). Furthermore, at several site-specific cases the El Niño 2009-10 winter erosion was at least three times as erosive as the previous most erosive winter when including both subaerial and bathymetric profile components (see Appendix B). Such significance of full profile analysis has been acknowledged in recent work that has extended the shoreline equilibrium model framework to full bathymetry profiles with credible success (Ludka et al., 2015).

Conceptually and numerically simple equilibrium shoreline models qualitatively reproduce observations of shoreline change. However, the model implements the initial equilibrium assumption with somewhat arbitrary functional forms (3.1-3.2), and bypasses modeling of the underlying complex physical processes. Extrapolation of equilibrium model predictions to wave conditions substantially beyond the calibration data set is therefore problematic. Within the calibration range, a single set of beach change model free parameters performed almost as well as parameters individually tuned for each beach section, providing a simple, generic shoreline change model for sandy reaches of this 90 km span.

Acknowledgements

This research was supported by the United States Army Corps of Engineers (W912HZ-14-2-0025) and the California Department of Parks and Recreation Division of Boating and Waterways (C1370032, program manager Reinhard Flick. San Diego Association of Governments (SANDAG), Coastal Frontiers Corporation, and Fugro are thanked for their assistance in using their data. André Doria was supported by Fellowships from the University of California Regents, National Defense Science & Engineering Graduate Fellowship (NDSEG), and the National Science Foundation Graduate Research Fellowships Program (GRFP). The statements, findings, conclusions and recommendations are those of the author(s) and do not necessarily reflect the views of the aforementioned organizations.

The text of Chapter 3, in full, is a reprint with minor modifications of the paper "Regional variability and modeling of Southern California beach sand levels," submitted for publication to *Continental Shelf Research*. The dissertation author was the primary researcher and first author with guidance provided by R.T. Guza and William C. O'Reilly.

Appendix A

Biannual Survey Timing

Monthly or more frequent subaerial beach surveys at Torrey Pines noted in Chapter 1 put the biannual San Diego County profiles, also analyzed in Chapter 1, in temporal context. The cross-shore location of the MSL contour (a proxy for subaerial volume change; Farris and List 2007) usually does not vary substantially over a few weeks, with the exception of the first winter storm (Figure A.1). Thus, the volume change results presented in Chapter 1 are generally insensitive to shifts of a few weeks in the survey timing. Figure A.1 also shows that the depth profiles analyzed, spaced roughly 6 months apart (fall and spring), do not necessarily correspond to seasonal extremes in beach width. For example, the surveys of May 2007 (eroded winter), Oct 2007 (accreted summer), and May 2008 (eroded winter) underestimate seasonal change. In those years the winter beach had already recovered by May, and the summer beach had eroded by October. In other years, the surveys are closer to seasonal extrema. The analysis in Chapter 1 examines the effect of profile truncation

on volume changes, irrespective of the underlying cross-shore and alongshore processes, or the precise timing of the profiles.

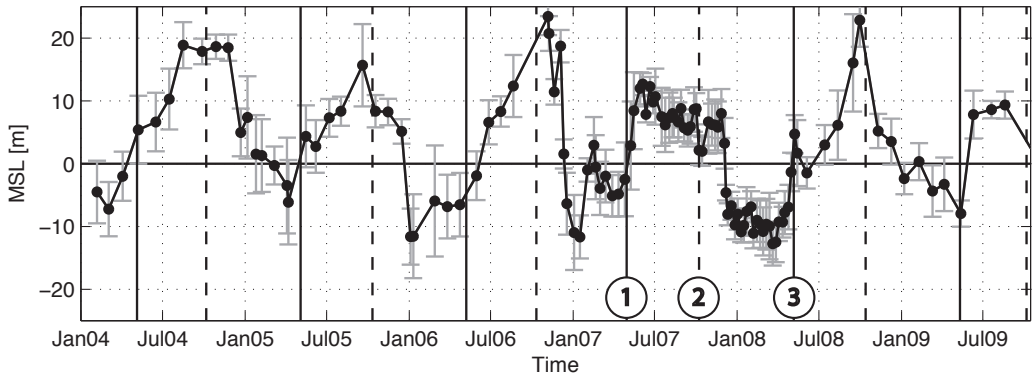

Figure A.1: Horizontal location of the MSL contour (mean removed) versus time at North Torrey Pines (see Figure 1.1) for ~6 years. Alongshore mean (black curve) and scatter bars (±1 standard deviation) are shown. Vertical black lines indicate San Diego County bathymetry survey dates (winter is solid; summer is dashed). Surveys, May 2007, October 2007, and May 2008, are labeled 1,2, and 3, respectively.

Appendix B

Cross-Shore Winter Profiles

During 2004-2013, beach sand levels on shore-normal transects spaced 100 m apart were surveyed quarterly from the back beach to ~8 m depth (Seymour et al., 2005) at four focus sites in San Diego County: Torrey Pines, Solana Beach, Cardiff, and Camp Pendleton (Figure 3.1a; 100 m spaced transects not shown). Average summer and winter cross-shore profiles were calculated on each cross-shore transect using the survey nearest in time to the subaerial beach summer accretion and winter erosion extremes. The difference between averaged winter and summer profiles shows the expected (e.g. Winant et al., 1975) displacement of sand from above MSL to an offshore bar (Figure B.1a,b). The most eroded winter survey shows erosion extending to 3.5 m depth, with the bar farther offshore (Figure B.1c). Winter profile anomalies are differences relative to the average winter profile (Figure B.1c,d). On transect j, the i*th* in time survey anomaly is

$$\tilde{d}_{ij}(x) = d_{ij}(x) - \left\langle d_{ij}(x) \right\rangle_i , \qquad \text{(B.1)}$$

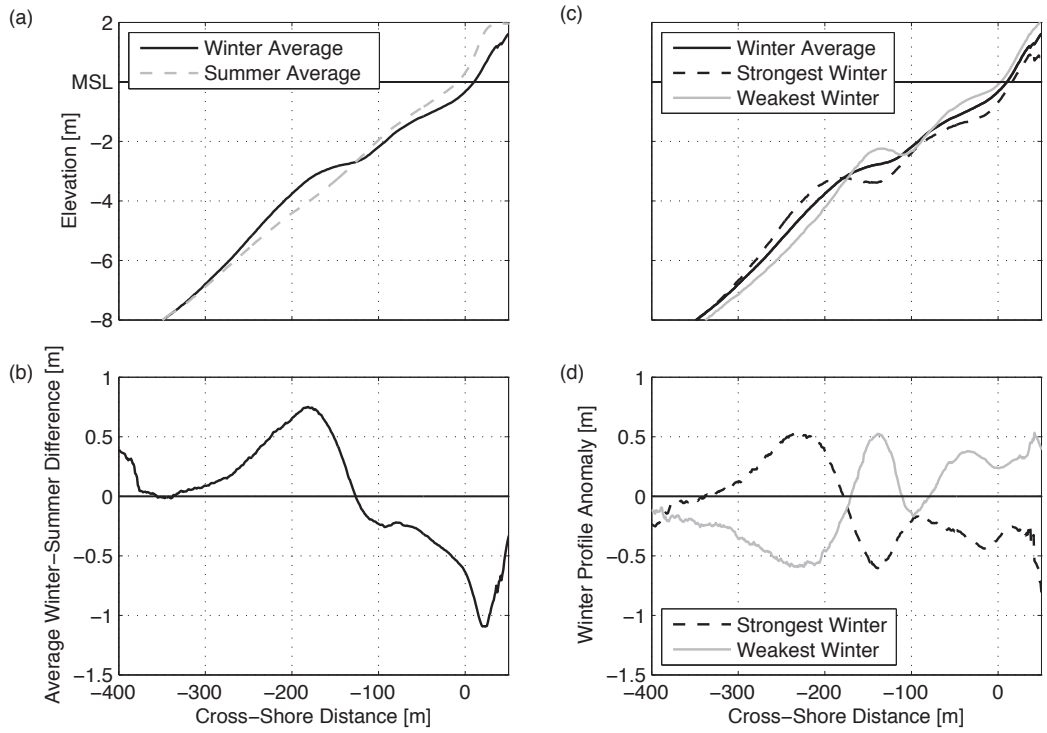

Figure B.1: Representative cross-shore transect at Torrey Pines. (a) Average winter (black) and summer (dashed gray) profiles and (b) difference between average winter and average summer profiles, (c) winter profiles: average, weakest (6 April 2009), and strongest (28 January 2010), and (d) strongest and weakest winter profile anomalies (e.g. deviation from the average winter profile).

with x the cross-shore coordinate, $d_{ij}(x)$ the cross-shore profile, and $\langle d_{ij}(x) \rangle_i$ the time-average of winter depth profiles on transect j. The profile anomaly of the strongest winter (difference from the average winter) has a shape similar to the difference between an average summer and average an winter (compare black dashed curve in Figure B.1d with black solid curve in Figure B.1b). Thus, the average winter profile is approximately midway between an average summer and an extreme winter. Most of the individual profile anomalies at Torrey Pines (Figure B.2) are

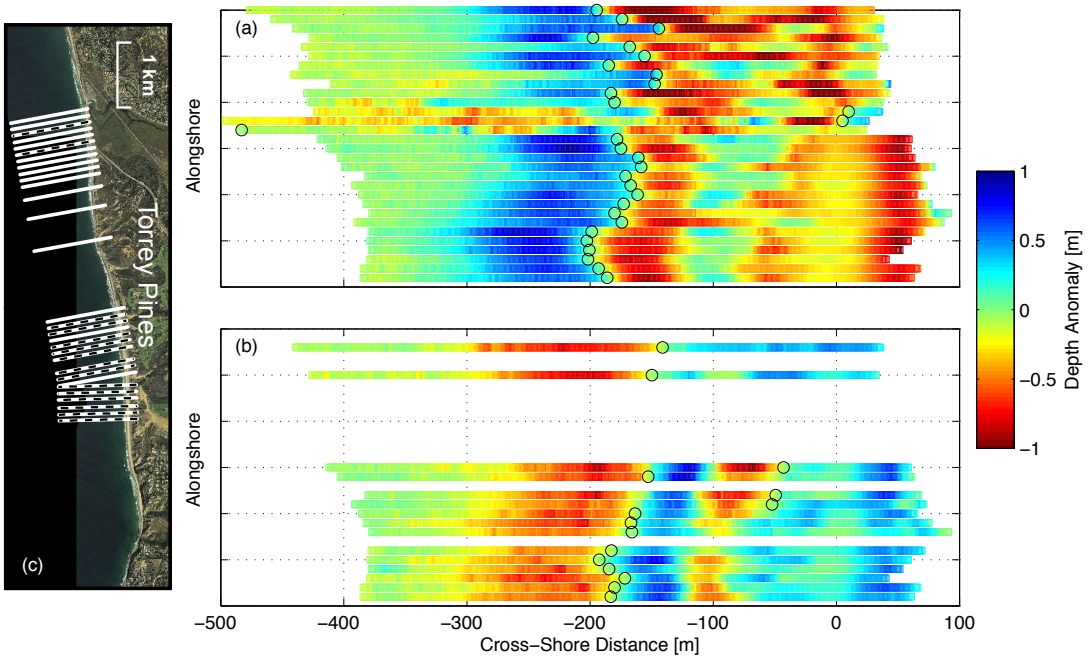

Figure B.2: Winter depth anomaly maps for a (a) strongest and (b) weakest winter at Torrey Pines. Depth anomaly transects for a given survey have been stacked and aligned so the cross-shore origin of each transect its average MSL position. Positive (negative) color bar values indicate anomalous accretion (erosion). Black circles show the pivot point location on each transect. Panel (c) transect lines show the locations of available transects stacked in (a) (all lines used) and (b) (only dashed lines used). Suboptimal tide and wave conditions during (b) caused data gaps in the surfzone larger than 20 m. These transects (blank in (b)) are excluded from analysis.

comparatively similar to the alongshore average (Figure B.1d). In strong winters, the bar is relatively strongly accreted (blue, x~-250m in Figure B.2a) and the shoreline is eroded (red). Conversely, weak winter anomalies (Figure B.2b) usually have an accretion deficit offshore, and higher relative shoreline sand levels (i.e. patterns of red-blue in Figures B.2a and B.2b are reversed).

The pivot point, $X_{p,ij}$, is the cross-shore boundary between regions of primarily anomalous erosion and accretion (black circles in Figure B.2a,b), and is defined as the cross-shore location that maximizes

$$p(x) = \left(\int_{X_{bb}}^{x} \tilde{d}(x')dx' \right)^2 + \left(\int_{x}^{X_{end}} \tilde{d}(x')dx' \right)^2, \quad \text{(B.2)}$$

where X_{bb} is the profile back beach or landward-most location, and X_{end} is the offshore profile extent location, and the ij indices are dropped. Alongshore variations of profile anomalies $\tilde{d}_{ij}(x)$ and pivot points $X_{p,ij}$ are usually weak (Figure B.2a,b).

B.1 Integrated profile anomalies

Cross-shore integrating the winter profile anomaly over the regions seaward and shoreward of X_p, and alongshore averaging over the number of surveyed transects (N) at a beach, yields the Integrated Profile Anomalies (IPA)

$$IPA_{shoreward} = \frac{1}{N} \sum_{j=1}^{N} \int_{X_{bb}}^{X_p} \tilde{d}_{ij}(x')dx' \quad \text{(B.3a)}$$

$$IPA_{seaward} = \frac{1}{N} \sum_{j=1}^{N} \int_{X_p}^{X_{end}} \tilde{d}_{ij}(x')dx' . \quad \text{(B.3b)}$$

At Torrey Pines during the weak 2008-09 winter, $IPA_{shoreward}$ was large and positive, indicating the upper beach was weakly eroded, and $IPA_{seaward}$ was large and negative, indicating reduced offshore bar deposition (Figure B.3a). The IPA signs during the 2008-09 winter were reversed relative to an erosive winter. The 2009-10 El Niño winter had the largest IPA magnitudes, both seaward and shoreward. If sand were conserved on each transect, with anomalously eroded beach face sand deposited in the offshore sandbar, $IPA_{seaward} = -IPA_{shoreward}$. However, during the 2010 El Niño, only about half the anomalous volume eroded from the beach face is found in the

enhanced offshore bar. The remainder may have been transported beyond the 8 m survey depth limit.

B.2 Erosion index

The Erosion Index (EI), a bulk measure of anomalous profile change, combines shoreward and seaward IPAs

$$EI = \frac{1}{2}\left(IPA_{seaward} - IPA_{shoreward}\right). \tag{B.4}$$

Positive EI indicates enhanced shoreline erosion and offshore bar accretion relative to the average winter (black curve in Figure B.3a). EI at Torrey Pines during the 2005-06 and 2007-08 winters was above average strength, and the 2009-10 El Niño winter was the most erosive. EI were remarkably similar at the four sites (Figure

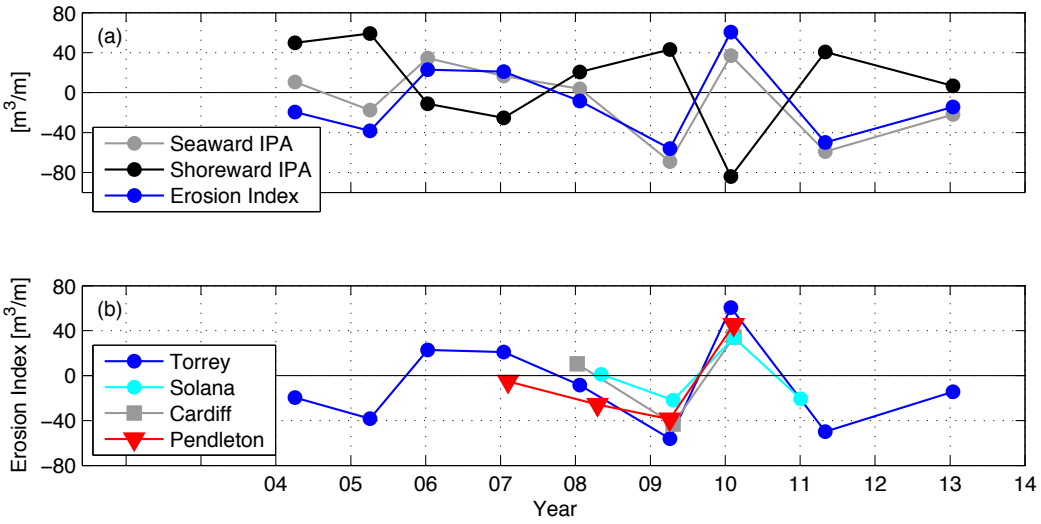

Figure B.3: (a) Integrated Profile Anomalies (IPA, see legend) and Erosion Index (EI, black curve) versus time (ticks are 1 January) at Torrey Pines, and (b) EI for all four focus beaches (see legend). There were no winter surveys in 2012. The number of 100-m spaced transects used to estimate IPA/EI are Torrey Pines (30), Solana Beach (13), Cardiff (14), and Camp Pendleton (20). All transects were not available in some surveys.

B.3b); the 2009-10 El Niño EI was at least ~3 times greater than the next most erosive winter at all beaches. The 2010-11 winter EI returned to near pre-El Niño 2009-10 EI levels, suggesting an efficient post-winter recovery of sand transported offshore.

References

Allan, J. C., and P. D. Komar (2002), Extreme storms on the Pacific Northwest Coast during the 1997–98 El Niño and 1998–99 La Niña, J. Coastal Res., 18(1), 175–193.

Allan, J. C., and P. D. Komar (2006), Climate controls on US West Coast erosion processes, *J. Coastal Res.*, 22(3), 511–529, doi:10.2112/03- 0108.1.

Aubrey, D. G. (1979). Seasonal patterns of onshore/offshore sediment movement. *Journal of Geophysical Research: Oceans*, *84*(C10), 6347-6354.

Aubrey, D. G., D. L. Inman, and C. D. Winant (1980), The statistical prediction of beach changes in southern California. *Journal of Geophysical Research: Oceans*, *85*(C6), 3264-3276.

Bamber, Jonathan L., Riccardo E. M. Riva, Bert L. A. Vermeersen, Anne M. LeBrocq (2009), Reassessment of the Potential Sea-Level Rise from a Collapse of the West Antarctic Ice Sheet, *Science*, 324(5929), 901-903, doi: 10.1126/science.1169335

Barnard, P. L., J. Allan, J. E. Hansen, G. M. Kaminsky, P. Ruggiero, and A. Doria (2011), The impact of the 2009-10 El Niño Modoki on U.S. West Coast beaches. *Geophys. Res. Lett.,* 38, doi: 10.1029/2011GL047707.

Barnard, P. L., A. D. Short, M. D. Harley, K. D. Splinter, S. Vitousek, I. L. Turner, J. Allan, M. Banno, K. R. Bryan, A. Doria, J. E. Hansen, Y. Kato, E. Randall-Goodwin, P. Ruggiero, I. J. Walker, and D. K. Heathfield (2015), Coastal vulnerability across the Pacific dominated by El Niño/Southern Oscillation. *Nature Geoscience*, *8*(10), 801-807.

Booker, A. J., J. E. Inman, P. D. Frank, D. B. Serafini, V. Torczon, and M. W. Trosset (1999), A rigorous framework for optimization of expensive functions by surrogates, *Struct. Multidiscip. Optim.*, 17(1), 1–13.

Brock, J.C., C. Wayne Wright, Asbury H. Sallenger, William B. Krabill and Robert N. Swift (2002), Basis and Methods of NASA Airborne Topographic Mapper Lidar Surveys for Coastal Studies, *J. Coastal Res.*, 18(1), 1-13.

Cai, W., S. Borlace, M. Lengaigne, P. Van Rensch, M. Collins, G. Vecchi, ... and M. H. England (2014), Increasing frequency of extreme El Niño events due to greenhouse warming. *Nature climate change*, *4*(2), 111-116.

Cai, W., G. Wang, A. Santoso, M. J. McPhaden, L. Wu, F. F. Jin, ... and M. H. England (2015), Increased frequency of extreme La Niña events under greenhouse warming. *Nature Climate Change*, *5*(2), 132-137.

California Department of Boating and Waterways and State Coastal Conservancy (2002), California Beach Restoration Study, Sacramento, California Department of Boating and Waterways and State Coastal Conservancy, Sacramento, Cali., http://www.dbw.ca.gov/PDF/Reports/BeachReport/FUll.pdf.

Castelle, Bruno, Vincent Marieu, Stéphane Bujan, Sophie Ferreira, Jean-Paul Parisot, Sylvain Capo, Nadia Sénéchal, and Thomas Chouzenoux (2014), Equilibrium shoreline modelling of a high-energy meso-macrotidal multiple-barred beach, *Marine Geology*, 347, 85–94, doi:10.1016/j.margeo.2013.11.003.

Coastal Frontiers Corporation (2002), SANDAG 2001 Regional Beach Monitoring Program annual report, Coastal Frontiers Corporation, Chatsworth, Cali., http://www.sandag.org/uploads/projectid/projectid_101_16641.pdf.

Coastal Frontiers Corporation (2016), SANDAG 2015 Regional Beach Monitoring Program Annual Report. [Available online at http://www.sandag.org/uploads/publicationid/2015beachsandmonitoringreport.zip]

Coastal Frontiers Corporation, 1997-2010: SANDAG Regional Beach Monitoring Program Annual Report, Chatsworth, CA.

Davidson, M. A., R. P. Lewis, and I. L. Turner (2010), Forecasting seasonal to multi-year shoreline change, *Coastal Engineering*, 57(6), 620-629, doi:10.1016/j.coastaleng.2010.02.001.

Davidson, M. A., K. D. Splinter, and I. L. Turner (2013), A simple equilibrium model for predicting shoreline change, *Coastal Engineering*, 73, 191–202, doi:10.1016/j.coastaleng.2012.11.002

Davis, R. E. (1976), Predictability of sea surface temperature and sea level pressure anomalies over the North Pacific Ocean. *Journal of Physical Oceanography*, *6*(3), 249-266.

Doria, A., and R. T. Guza (2013), Estimating Changes in Near-Shore Bathymetry with Subaerial Surveys. *Journal of Atmospheric and Oceanic Technology*, *30*(9), 2225-2232.

Doria, A., R. T. Guza, W C. O'Reilly, and M. L. Yates (2016), Observations and modeling of San Diego beaches during El Niño. *Continental Shelf Research*. 124, 153-164.

Dyurgerov, Mark B., and Mark F. Meier (2000), Twentieth century climate change: Evidence from small glaciers, *Proceedings of the National Academy of Sciences*, 97(4), 1406-1411.

Everts, C. H. and C. D. Eldon (2005), Sand capture in Southern California submarine canyons. *Shore and beach*, (1), 3-11.

Farris, A. S., and J. H. List (2007), Shoreline Change as a Proxy for Subaerial Beach Volume Change. *J. Coastal Res.,* 23, 740-748.

Flick, Reinhard E., and B.Walton Waldorf (1984), Performance documentation of the Longard Tube at Del Mar, California 1980–1983, *Coastal Engineering*, 8(3), 199-217, doi:10.1016/0378-3839(84)90001-2.

Gallien, T.W., J.E. Schubert, and B.F. Sanders (2011), Predicting tidal flooding of urbanized embayments: A modeling framework and data requirements, *Coastal Engineering*, 58(6), 567-577, doi:10.1016/j.coastaleng.2011.01.011.

Gallien, T. W., W. C. O'Reilly, R. E. Flick, and R. T. Guza (2015), Geometric properties of anthropogenic flood control berms on southern California beaches. *Ocean & Coastal Management*, *105*, 35-47.

Gares, P. A., Y. Wang, and S. A. White (2006), Using LIDAR to monitor a beach nourishment project at Wrightsville Beach, North Carolina, USA.*Journal of Coastal Research*, 1206-1219.

Graham, N. E., and H. F. Diaz (2001), Evidence for intensification of North Pacific winter cyclones since 1948, *Bull. Am. Meteorol. Soc.*, 82, 1869–1893, doi:http://dx.doi.org/10.1175/1520-0477(2001)082<1869:EFIONP>2.3. CO;2.

Griggs, G. B., K. Patsch, and L. E. Savoy (2005), *Living with the changing California coast*. Univ of California Press.

Inman, D. L., and B. M. Brush (1973), The coastal challenge. *Science*, *181*(4094), 20-32.

Johnson, Bradley D., Nobuhisa Kobayashi, and Mark B. Gravens (2012), Cross-Shore Numerical Model CSHORE for Waves, Currents, Sediment Transport and Beach Profile, ERDC/CHL TR-12-22, Coastal and Hydraulics Lab. (U.S.) Eng. Res. and Dev. Center (U.S.), Vicksburg, Miss.

Keeling, C. D., T. P. Whorf, M. Wahlen, and J. Van Der Plichtt (1995), *Nature*, 375, 666-670, doi: 10.1038/375666a0.

Komar, P. D., and D. L. Inman (1970), Longshore sand transport on beaches.*Journal of geophysical research*, *75*(30), 5914-5927.

Kradill, W. B., C. W. Wright, J. C. Brock, R. N. Swift, E. B. Frederick, S. S. Manizade,, ... and W. Hulslander (1997), Airborne Laser/GPS Mapping of Assateague National Seashore Beach.

Larson, M., and N. C. Kraus (1989), SBEACH: Numerical model for simulating storm-induced beach change, Tech. Rep. CERC-89-9, U.S. Army Corps of Eng., Vicksburg, Miss.

Long, T. M., J. Angelo, and J. F. Weishampel (2011), LiDAR-derived measures of hurricane- and restoration-generated beach morphodynamics in relation to sea turtle nesting behaviour. *Int. J. Remote Sens.,* 32, 231-241.

Ludka, B. C., R. T. Guza, W. C. O'Reilly, and M. L. Yates (2015), Field Evidence of Beach Profile Evolution Towards Equilibrium, *J. Geophys. Res. Oceans*, 120, doi:10.1002/2015JC010893.

Marsden, A. L., M. Wang, J. E. Dennis, and P. Moin (2004), Optimal aerocoustic shape design using the surrogate management framework, *Optim. Eng.*, 5(2), 235–262.

McLachlan, A., and A. Brown (2010), The Ecology of Sandy Shores, Academic Press, Burlington, Mass.

Miller, Jon K., and Robert G. Dean (2004), A simple new shoreline change model, *Coastal Eng.*, 51(7), 531–556, doi:10.1016/j.coastaleng.2004.05.006.

Moore, L. J., B. T. Benumof, and G. B. Griggs (1999), Coastal Erosion Hazards in Santa Cruz and San Diego Counties, California. *J. Coastal Res.,* SI, 121-139.

Nicholls, R. J., P. P. Wong, V. R. Burkett, J. O. Codignotto, J. E. Hay, R. F. McLean, S. Ragoonaden, and C. D. Woodroffe (2007), Coastal systems and low-lying areas. *Climate Change 2007: Impacts, Adaptation and Vulnerability. Contribution of Working Group II to the Fourth Assessment Report of the Intergovernmental Panel on Climate Change*, Cambridge University Press, Cambridge, UK, 315-356.

Nordstrom, C. E., and D. L. Inman (1975), Sand level changes on Torrey Pines Beach, California, (U.S.) Coastal Eng. Res. Center, Fort Belvoir, Virg.

O'Reilly, W.C. and R.T. Guza (1991), Comparison of spectral refraction and refraction-diffraction wave models, *J. Waterway, Port, Coastal, and Ocean Engineering*, 117, 199-215.

O'Reilly, W.C., and R.T. Guza (1993), A comparison of spectral wave models in the Southern California Bight, *Coastal Eng.*, 19, 263-282.

O'Reilly, W.C., and R.T. Guza (1998), Assimilating coastal wave observations into regional swell predictions. Part I: Inverse methods, *J. Phys. Oceanogr.*, 28, 679-691.

O'Reilly, W. C., C. B. Olfe, J. Thomas, R. J. Seymour, and R. T. Guza (2016), The California coastal wave monitoring and prediction system. *Coastal Engineering*, *116*, 118-132.

Patsch, K., and G. Griggs (2006), *Littoral cells, sand budgets, and beaches: understanding California's shoreline*. Institute of Marine Sciences, University of California, Santa Cruz.

Pawka, S. S. (1983), Island shadows in wave directional spectra, *J. Geophys. Res.*, 88(C4), 2579–2591, doi:10.1029/JC088iC04p02579.

Pfeffer, W. T., J. T. Harper, and S. O'Neel (2008), Kinematic constraints on glacier contributions to 21st-century sea-level rise, *Science*, 321, 1340–1343, doi:10.1126/science.1159099.

Press, W. H., S. A. Teukolsky, W. T. Vetterling, and B. P. Flannery (2007), *Numerical recipes 3rd edition: The art of scientific computing*. Cambridge University Press.

Rahmstorf, Stefan, Anny Cazenave, John A. Church, James E. Hansen, Ralph F. Keeling, David E. Parker, and Richard C. J. Somerville (2007), Recent Climate Observations Compared to Projections, *Science*, 316, doi: 10.1126/science.1136843.

Reineman, B. D., L. Lenain, D. Castel, and W. K. Melville (2009), A portable airborne scanning lidar system for ocean and coastal applications. *Journal of Atmospheric and oceanic technology*, *26*(12), 2626-2641.

Revell, David L., Paul D. Komar, and Asbury H. Sallenger Jr. (2002), An Application of LIDAR to Analyses of El Niño Erosion in the Netarts Littoral Cell, Oregon, J. Coastal Res., 18(4), 792-801.

Revell, D. L., J. E. Dugan, and D. M. Hubbard (2011), Physical and Ecological Responses of Sandy Beaches to the 1997-98 El Niño. *J. Coastal Res.,* 27, 718-730.

Roelvink, Dano, Ad Reniers, Ap van Dongeren, Jaap van Thiel de Vries, Robert McCall, and Jamie Lescinski (2009), Modelling storm impacts on beaches, dunes and barrier islands, *Coastal Eng.*, 56, 1133-1152, doi:10.1016/j.coastaleng.2009.08.006.

Ruggiero, Peter, P. D. Komar, and J. C. Allan (2010a), Increasing wave heights and extreme-value projections: The wave climate of the U.S. Pacific Northwest, *Coastal Eng.*, 57, 539–552, doi:10.1016/j.coastaleng. 2009.12.005.

Ruggiero, Peter, Maarten Buijsman, George M. Kaminsky, and Guy Gelfenbaum (2010b), Modeling the effects of wave climate and sediment supply variability on large-scale shoreline change, *Marine Geology*, 273, 127-140.

Sallenger, A. H., W. Krabill, J. Brock, R. Swift, S. Manizade, and H. Stockdon (2002), Sea-cliff erosion as a function of beach changes and extreme wave runup during the 1997-1998 El Niño. *Mar. Geol.,* 187, 279-297.

Sallenger, A. H., W. B. Krabill, R. N. Swift, J. Brock, J. List, M. Hansen, R. A. Holman, S. Manizade, J. Sontag, A. Meredith, K. Morgan, J. K. Yunkel, E. B. Frederick, and H. Stockdon (2003), Evaluation of Airborne Topographic Lidar for Quantifying Beach Changes. *J. Coastal Res.,* 19, 125-133.

Sallenger, A. H., H. Stockdon, J. Haines, W. Krabill, R. Swift, and J. Brock (2004), Probabilistic assessment of beach and dune changes. In *Coastal Engineering 2000-27th International Conference on Coastal Engineering, ICCE 2000* (Vol. 276, pp. 3035-3047).

Seymour, R., R. T. Guza, W. O'Reilly, and S. Elgar (2005), Rapid erosion of a small southern California beach fill. *Coastal Eng.,* 52, 151-158.

Shepard, F.P. (1950), Beach cycles in southern California, Tech. Memo 20, Beach Erosion Board, U.S. Army Corps of Engineers, Washington, D.C.

Splinter, K.D., I. L. Turner, and M. A. Davidson (2013), How much data is enough? The importance of morphological sampling interval and duration for calibration of empirical shoreline models, *Coastal Eng.*, 77, 14-27, doi:10.1016/j.coastaleng.2013.02.009.

Splinter, K. D., I. L. Turner, M. A. Davidson, P. Barnard, B. Castelle, and J. Oltman-Shay (2014), A generalized equilibrium model for predicting daily to interannual shoreline response, *J. Geophys. Res.*, 119, 1936–1958, doi:10.1002/2014JF003106.

Stockdon, H. F., A. H. Sallenger, J. H. List, and R. A. Holman (2002), Estimation of shoreline position and change using airborne topographic lidar data. *Journal of Coastal Research*, 502-513.

Stockdon, H. F., K. S. Doran, and A. H. Sallenger (2009), Extraction of lidar-based dune-crest elevations for use in examining the vulnerability of beaches to inundation during hurricanes. *Journal of Coastal Research*, 59-65.

Storlazzi, C. D., and M. E. Field (2000), Sediment distribution and transport along a rocky, embayed coast: Monterey Peninsula and Carmel Bay, California. *Marine Geology*, *170*(3), 289-316.

Thomas, T., M. R. Phillips, A. T. Williams, and R. E. Jenkins (2011), Short-term beach rotation, wave climate and the North Atlantic Oscillation (NAO).*Progress in Physical Geography*, *35*(3), 333-352.

Vermeer, M., and S. Rahmstorf (2009), Global sea level linked to global temperature, Proc. Natl. Acad. Sci. U. S. A., 106(51), 21527-21532, doi:10.1073/pnas.0907765106.

Warrick, J.A., K. Rosenberger, A. Lam, J. Ferreira, I. M. Miller, M. Rippy, J. Svejkovsky, and N. Mustain (2012), Observations of coastal sediment dynamics of the Tijuana Estuary Fine Sediment Fate and Transport Demonstration Project, Imperial Beach, California, U.S. Geological Survey, Open-File Report 2012–1083, http://pubs.usgs.gov/of/2012/1083/.

Winant, C. D., D. L. Inman, and C. E. Nordstrom (1975), Description of seasonal beach changes using empirical eigenfunctions, *J. Geophys. Res.*, 80, 1979–1986.

Wright, L.D, A.D Short, and M.O Green (1985), Short-term changes in the morphodynamic states of beaches and surf zones: An empirical predictive model, *Marine Geology*, 62, 339-364, doi:10.1016/0025-3227(85)90123-9.

Yang, B., M. Madden, J. Kim, and T. R. Jordan (2012), Geospatial analysis of barrier island beach availability to tourists. *Tourism Manage.,* 33, 840-854.

Yates, M.L., R. T. Guza, Roberto Gutierrez, and Richard Seymour (2008), A Technique for Eliminating Water Returns from Lidar Beach Elevation Surveys, J. Atmos. *Oceanic Technol.*, 25, 1671–1682, doi:10.1175/2008JTECHO561.1.

Yates, M. L., R. T. Guza, and W. C. O'Reilly (2009a), Equilibrium shoreline response: Observations and modeling. *J. Geophys. Res.,* 114, doi:10.1029/2009JC005359.

Yates, M. L., R. T. Guza, W. C. O'Reilly, and R. J. Seymour (2009b), Overview of seasonal sand level changes on southern California beaches. *Shore & Beach,* 77, 39-46.

Yates, M. L., R. T. Guza, W. C. O'Reilly, and R. J. Seymour (2009c), Seasonal persistence of a small southern California beach fill, *Coastal Eng.*, 56, 559-564, doi:10.1016/j.coastaleng.2008.11.004.

Yates, M. L., R. T. Guza, W. C. O'Reilly, J.E. Hansen, and P. L. Barnard (2011), Equilibrium shoreline response of a high wave energy beach, *J. Geophys. Res.*, 116, doi: 10.1029/2010JC006681.

Young, A. P., and S. A. Ashford (2006), Application of airborne LIDAR for seacliff volumetric change and beach-sediment budget contributions. *Journal of Coastal Research*, 307-318.

Young, A. P., J. H. Raymond, J. Sorenson, E. A. Johnstone, N. W. Driscoll, R. E. Flick, and R. T. Guza (2010), Coarse Sediment Yields from Seacliff Erosion in the Oceanside Littoral Cell. *J. Coastal Res.,* 26, 580-585.

Young, A. P., R. T. Guza, P. N. Adams, W. C. O'Reilly, and R. E. Flick (2012), Cross-shore decay of cliff top ground motions driven by local ocean swell and infragravity waves, *J. Geophys. Res.*, 117, doi:10.1029/2012JC007908.

Zhang, Keqi, Bruce C. Douglas, and Stephen P. Leatherman (2004), Global warming and coastal erosion, *Climatic Change*, 64, 41-58.